

Crumbling Crystals: On the Dissolution Mechanism of NaCl in Water

Niamh O'Neill and Stephen J. Cox

Yusuf Hamied Department of Chemistry, University of Cambridge, Lensfield Road, Cambridge, CB2 1EW, UK

Christoph Schran* and Angelos Michaelides†

Yusuf Hamied Department of Chemistry, University of Cambridge,
Lensfield Road, Cambridge, CB2 1EW, UK and

Thomas Young Centre, London Centre for Nanotechnology,
and Department of Physics and Astronomy, University College London,
Gower Street, London, WC1E 6BT, United Kingdom

Life on Earth depends upon the dissolution of ionic salts in water, particularly NaCl. However, an atomistic scale understanding of the process remains elusive. Simulations lend themselves conveniently to studying dissolution since they provide the spatio-temporal resolution that can be difficult to obtain experimentally. Nevertheless, the complexity of various inter- and intra-molecular interactions require careful treatment and long time scale simulations, both of which are typically hindered by computational expense. Here, we use advances in machine learning potential methodology to resolve for the first time at an *ab initio* level of theory the dissolution mechanism of NaCl in water. The picture that emerges is that of a steady ion-wise unwrapping of the crystal preceding its rapid disintegration, reminiscent of crumbling. The onset of crumbling can be explained by a strong increase in the ratio of the surface to volume of the crystal. Overall, dissolution is comprised of a series of highly dynamical microscopic sub-processes, resulting in an inherently stochastic mechanism. These atomistic level insights now pave the way for a general understanding of dissolution mechanisms in other crystals, and the methodology is primed for more complex systems of recent interest such as water/salt interfaces under flow and salt crystals under confinement.

I. INTRODUCTION

Understanding the dissolution of crystals is vital for a myriad of pressing modern day challenges, from technological issues such as battery science [1] and water desalination [2] to drug bioavailability [3] and geochemical weathering [4]. The macroscopic process of dissolution is well described and understood from thermodynamics, where enthalpies of dissolution for example can be readily obtained from experimental techniques such as calorimetry [5]. However despite well understood general theories describing the conceptually reverse process of nucleation [6], at a microscopic level our understanding of dissolution remains largely unresolved.

Dissolution is indeed an old problem [7], however with recent experimental developments, it is an exciting time for the field. Building on early atomic force microscopy studies of the water/NaCl interface by Xu et al. [8], sophisticated imaging techniques such as scanning tunneling microscopy [9] and Bragg coherent diffraction imaging [10] have given insight into low temperature surface ion dissolution events and the role of defects in the dissolution process. In addition, recent impressive high-resolution liquid cell transmission electron microscopy work has observed defect-mediated ripening of Cd-CdCl₂ core-shell nanoparticles [11]. The solid-liquid interface under flow has also been probed with a combination of surface-specific sum frequency generation spectroscopy

and microfluidics experiments, revealing drastic changes to the equilibrium of dissolved ions.[12] Recent single-molecule atomic-resolution real-time electron microscopy experiments have captured in real time a NaCl nucleus emerging during nucleation [13] while atomic electron tomography has been used to monitor the nucleation of FePt nanoparticles over time [14]. However in general, obtaining atomic scale dynamical information from experiment remains a highly challenging endeavour.

In contrast, computer simulations conveniently grant access to the Ångstrom and femtosecond scale resolution required, and have been applied to study the dissolution of a range of materials (see e.g. refs 15–23). Important insights have been obtained from these simulations that have significantly advanced the field, such as the fact that dissolution rates are highly controlled by the crystal structure, and that the existence of site specific barriers to dissolution implies a non-constant dissolution rate throughout the process [24–28]. Nevertheless, simulation studies up to now have had limitations. Notably, both force field (FF) and *ab initio* studies have been limited to individual trajectories of dissolution events. However, a stochastic dissolution process is expected, as shown for example in larger scale studies in the geosciences [29]. Therefore it is important to establish if the sequence of dissolving atoms can be rationalised at an atomistic level from an ensemble of dissolution trajectories. In addition, nucleation pathways are strongly dependent on solution concentration [30–32], raising the question whether dissolution follows the same predictable mechanism or if it is highly sensitive to the conditions.

The questions noted above highlight the need for com-

* cs2121@cam.ac.uk

† am452@cam.ac.uk

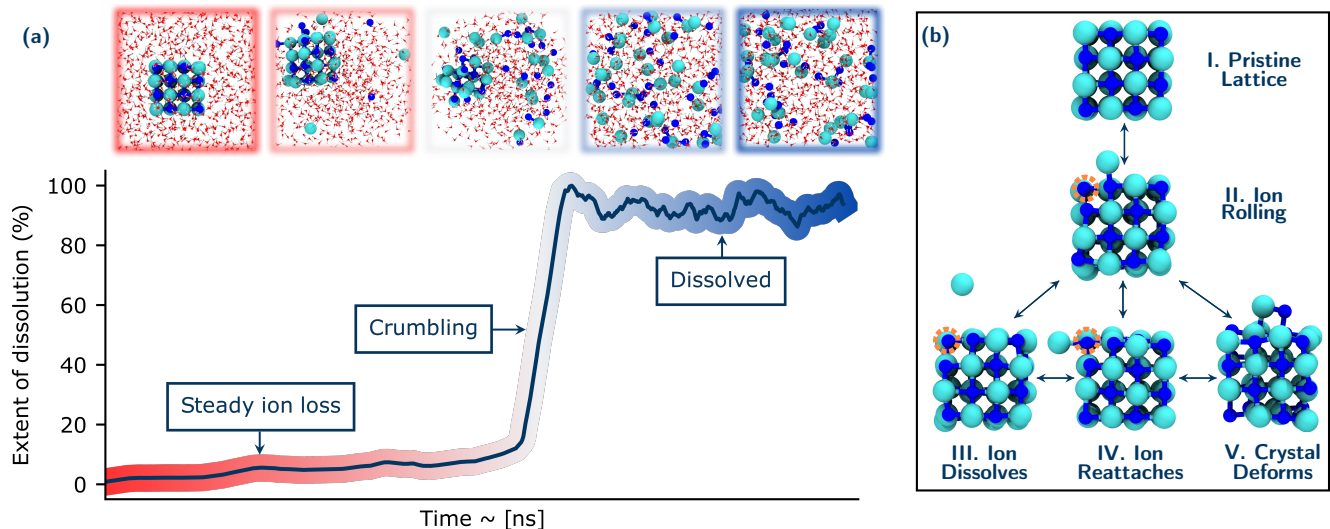


FIG. 1. **Overview of the NaCl dissolution process for a typical nanocrystal dissolution event.** Panel (a) shows the extent of dissolution of a NaCl nanocrystal in water, which involves a steady loss of ions followed by a rapid crumbling event. Relevant snapshots along the trajectory are shown above the plot. Na^+ and Cl^- ions are coloured in blue and cyan respectively and oxygen and hydrogen atoms are coloured in red and white, respectively. (b) Sub-processes occurring during the dissolution. The vacancies left by the ions moving are shown by the orange circles. For clarity in panel (b) the water molecules present in the simulation cell are not shown.

putationally efficient explorations of multiple dissolution trajectories using a methodology that accurately describes the delicate changes in water-water and water-ion interactions that occur during dissolution. Fortunately, with the emergence of machine learning interatomic potentials (MLPs) [33–36], accurate and efficient potentials can be developed for the treatment of complex processes such as dissolution. Such potentials yield the accuracy of *ab initio* methods but at a fraction of the computational cost. Of the many flavours of MLP methodology, the approach reported in ref. 37 is particularly suitable as it enables the automated development and validation of MLPs capable of accurately treating complex aqueous systems.

Given the opportunities presented by the recent developments in MLP technology, we have performed a detailed study of NaCl dissolution. NaCl dissolution is a prototypical and widely studied system [38–48], because of its ubiquity and significance to phenomena including biological intracellular reactions [49] and climate chemistry [50, 51], not forgetting that two-thirds of the Earth is covered in salty water. We find that the dissolution process is highly dynamic. Many stochastic sub-processes combine to give an overall crumbling mechanism, in which a steady period of ion-wise dissolution precedes the rapid concerted disintegration of the crystal. This disintegration is governed by the steep increase of the surface to volume ratio of the crystal, corresponding to an unfavourable surface to bulk free energy – borrowing from ideas of classical nucleation theory (CNT) – that ultimately leads to the rapid collapse of the crystal.

II. THE NaCl DISSOLUTION MECHANISM

Figure 1 provides an overview of a prototypical system considered and the NaCl dissolution process. Throughout this discussion, we show representative trajectories at one temperature but the phenomena observed hold for multiple trajectories at 330 K and 400 K. Full details of the systems and simulation protocols are given in the Methods section. However, in brief, we considered 64 and 216 ion NaCl nanocrystals in simulation boxes containing 1250 to 625 water molecules (giving NaCl concentrations when dissolved of 1.42, 2.84 and 5.61 mol/kg). While we have not computed the solubility of the ML model, the experimental saturation of NaCl in water is 6.15 mol/kg. All systems explored started out with a NaCl nanocrystal in pure water and the final dissolved state is likely undersaturated or at worst at a low supersaturation, thereby facilitating the complete dissolution of the crystal. A typical dissolution trajectory is shown in Figure 1 (a), with the extent of dissolution of the crystal monitored over time. Relevant snapshots from the trajectory are shown in the upper panel. After a steady period corresponding to ions dissolving from typically low coordinated sites of the crystal into solution, there is a rapid increase in the rate of dissolution. This suggests the crystal reaches some critical point of instability after which it rapidly disintegrates or crumbles. Following this, the Cl^- and Na^+ ions are fully solvated and the system has lost all crystalline order. These general observations for the dissolution mechanisms are consistent over all conditions studied and reproducible over the ensemble of trajectory-

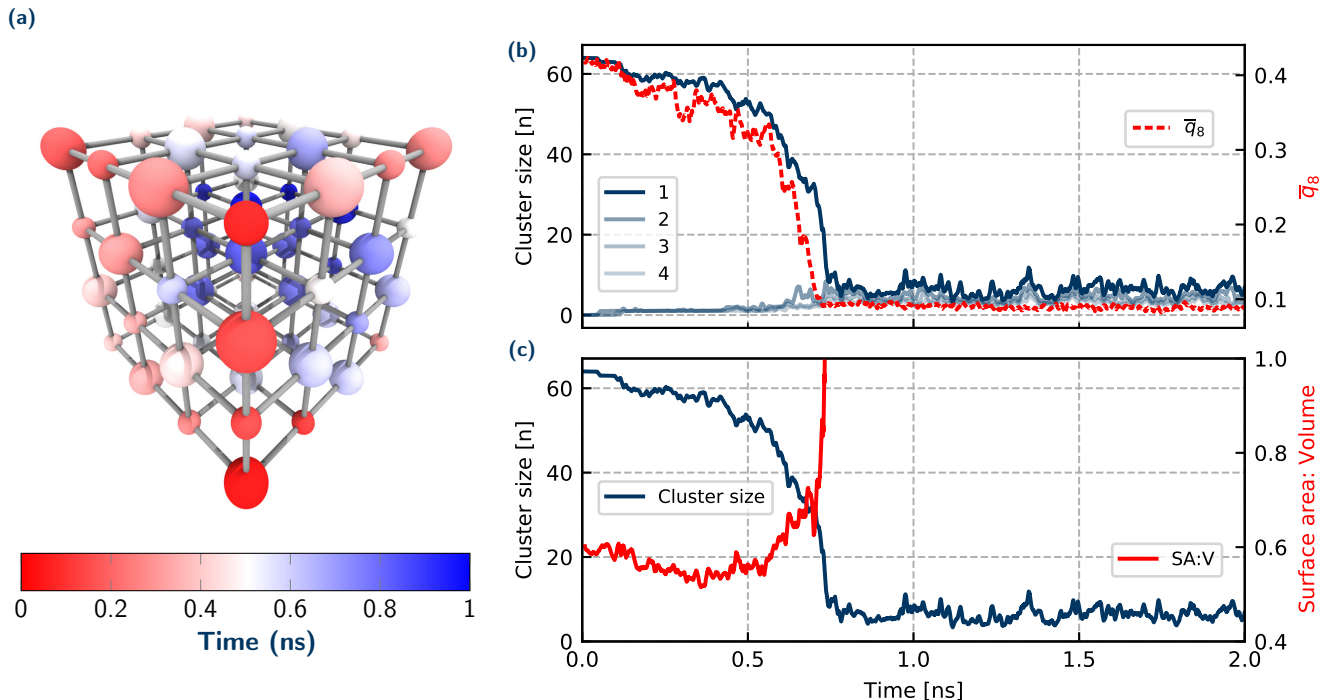


FIG. 2. **Summary of crystal and system properties for a dissolution trajectory at 2.42 mol/kg.** (a) Time taken for individual ions to dissolve in a representative NaCl nano-crystal, where the larger ions are Cl^- and smaller ions are Na^+ . Evolution over time of (b) cluster size of 4 largest ionic clusters and crystalline order parameter \bar{q}_8 (c) the ratio of surface area to volume (red, SA:V) of largest cluster (blue).

ries at a given condition.

The early stages of dissolution up to the onset of crumbling comprise a set of dynamic processes occurring in equilibrium as shown in Figure 1 (b). The dissolution of any ion from the crystal is first preceded by the ion rolling onto the surface of the crystal (Structures I. & II.). This process involves a simultaneous reduction in coordination of the rolling ion with its neighbours in the lattice until it is just coordinated with one counter ion, and a corresponding increase in coordination of the ion with water. This behaviour is consistent with earlier AIMD studies on NaCl and $\text{Li}_x\text{Mn}_2\text{O}_4(001)$ surfaces. [40, 52] Moreover, there is a difference between the rolling behaviour of Na^+ and Cl^- : Na remains much more stable on the surface, while Cl^- is much quicker to dissolve into solution. This is in agreement with recent work by Silvestri et al. [15], in which they show that Na^+ ions are stable on terrace sites when they move from kink sites, while Cl^- has much weaker minima on terrace sites. There are then several possibilities for the fate of this exposed ion: It can become further solvated by water and completely dissolve from the crystal (Structure III.) It can also roll back to its starting position and/or further roll to an orthogonal face (where it again has the possibility to dissolve from the crystal) (Structure IV.). The dissolved ion can also re-join the crystal (at not necessarily the same location as it originally emerged). In these early stages before the rapid

collapse of the crystal, other ions can also simultaneously roll and move about the crystal without necessarily any dissolution. This results in a deformation of the crystal shown in Structure V. The implications of these early dynamic processes with respect to the stochastic nature of dissolution will be discussed in detail in Section III.

Figure 2 (a) shows a schematic of the typical ‘unwrapping’ of the crystal. The ions are coloured according to their time taken to dissolve. Overall there is a preference for ions from low coordinated sites to dissolve first. We observe that dissolution is initiated at corner sites in the lattice, which has been previously noted in several papers [38, 40, 41, 47, 53]. The dissolution of ions up to the point of crumbling proceeds in an approximately step-wise manner of ions of opposite charge (Cl^- , Na^+ , Cl^- ...), thereby minimising charge accumulation on the crystal lattice, confirming earlier force-field simulations on the initial stages of dissolution [47]. At each dissolution step (depending on its location) for an ion to dissolve it must break 3 (corner), 4 (edge), 5 (face) or 6 (centre) ionic bonds. Therefore the edge-wise unwrapping of the crystal shown in Figure 2 (a) follows the hypothesis that at each step, the number of ionic bonds broken is minimised. This holds true up to the point of rapid disintegration, where all atoms irrespective of their current coordination dissolve within a few picoseconds.

These initial observations raise numerous questions re-

garding details of the crumbling mechanism proposed. Specifically: (i) Does the crystal splinter into smaller crystallites or completely crumble into ions? (ii) Nucleation studies of NaCl in water, have shown that at very high concentrations there is an amorphous ionic structure before ions from solution form a nucleus [30, 31]. Therefore is there also evidence for an amorphous intermediate before the complete dissolution of the crystal? (iii) At what point does the crystal disintegrate, and is this crumbling event determined by the size of the remaining crystalline cluster or something else?

To answer these questions, we now analyse the nature of the crumbling mechanism, and attempt to quantify and describe the driving force for this event. Let us first address the question whether the remaining crystal splinters into smaller subclusters which is suggested in Ref. 41. Another possibility is that it rapidly crumbles into individual ions. Monitoring the sizes of the 4 largest crystalline (ionic) clusters and the crystalline order of the largest cluster over time, as shown in Figure 2 (b) gives insight into the exact mechanism of the crystal collapse. Considering the sizes of the 4 largest ionic clusters, initially there is just one large cluster with 64 ions (i.e. the initial $4 \times 4 \times 4$ crystal), which gradually decreases in size corresponding to the steady period of ions dissolving. At the point of crumbling, the number of ions in the largest cluster rapidly drops and immediately converges to a steady value of just one or two ions rapidly fluctuating over time (corresponding to short-lived ion pairs in solution). Since at no stage is there a second cluster with some intermediate number of ions, this implies that there is a complete disintegration of the crystal, rather than something resembling a shattering process.

To understand if an amorphous transition precedes crumbling, the crystalline order of the ions in the system has been monitored over time. \bar{q}_8 (defined in the SI) is a variation of the typical Steinhardt bond order parameter q_8 , and averages the bond order vectors over the first shell of neighbouring ions to provide a measure of ordering of the ions in the system. \bar{q}_8 (Figure 2 (b)) qualitatively tracks the evolution of the largest cluster size, whereby initially there is a steady decrease (but still within the range expected for a crystal) corresponding to the crystal decreasing in size. At a critical value of $\bar{q}_8 \approx 0.3$, there is a sharp decrease in \bar{q}_8 , corresponding to a rapid total loss of crystalline order in the system. Therefore for the (low) concentration regimes we explore, our results are in agreement with the nucleation literature, where there is a single step order to disorder transition, with no amorphous intermediate.

We have already suggested that the onset of crumbling occurs when the crystal reaches a critical point of instability. Across the simulated trajectories, there is a wide spread of crystal sizes at which the disintegration occurs (approximately 20-40 ions). So it is not size alone that governs the instability of the nanocrystal. To understand this behaviour we considered the surface area to volume ratio of the convex hull of the largest cluster. Panel (c)

in Figure 2 shows this surface area to volume ratio for the crystal over time up to the point of collapse. This gives a measure of the extent of interaction of the ions in the crystal with water over time. There is an initial decrease corresponding to a ‘rounding’ of the crystal, to a relatively constant value up to the point of crumbling. (This rounding is even more pronounced for the larger $6 \times 6 \times 6$ crystal, Figure S10.) At the onset of crumbling there is then a rapid increase in the surface area accessible to the water. Our system is not in a concentration regime where reversible dissolution and nucleation is to be expected. However, with this ratio we can draw direct parallels with CNT. Within CNT, the free energy of formation of a crystal nucleus comprises a volume term representing the gain in free energy upon formation of a stable crystalline phase, and an unfavourable surface term arising from the cost of forming an interface. The dominance of the surface area over the volume at the point of crumbling of the crystal lattice in this dissolution work is akin to a rapid increase in the (destabilising) surface free energy in CNT. Therefore there is a delicate balance of intra- and inter-molecular interactions that ultimately determine the crystal stability.

We note that the cluster at the point of crumbling here is not equivalent to a critical nucleus in CNT. For the concentration regimes explored here, the critical nucleus would be expected to be much larger [30]. To further test the robustness of our proposed crumbling mechanism, we performed simulations on the same systems using the Joung Cheatham force field for ion-ion interactions with the SPC/E water model [54]. This has a computed solubility of 3.7 mol/kg, and therefore we can be sure that our systems are below saturation when fully dissolved for this model. Full details and results are given in the SI, however we observe qualitatively the same crumbling mechanism, with similar cluster sizes at the point of crumbling. Therefore despite not having the solubility of the ML model, we can be confident that this mechanism is not simply a reverse of CNT.

In summary, this ratio is a simple parameter that explains the onset of disintegration of the crystal. It can also be used directly for other systems, thereby allowing for a simple and intuitive understanding of dissolution processes in general.

III. STOCHASTIC NATURE OF THE NaCl DISSOLUTION PROCESS

Thus far, we have described the overall crumbling mechanism of NaCl dissolution in detail, which is completely general for multiple conditions of concentration and temperature. However a pertinent question relevant for many fields is whether the dissolution mechanism is deterministic. That is, given some initial conditions, can we predict at what crystal size/structure and after how long will the crystal dissolve? Previous *ab initio* studies [40, 41] and larger scale FF-based studies on disso-

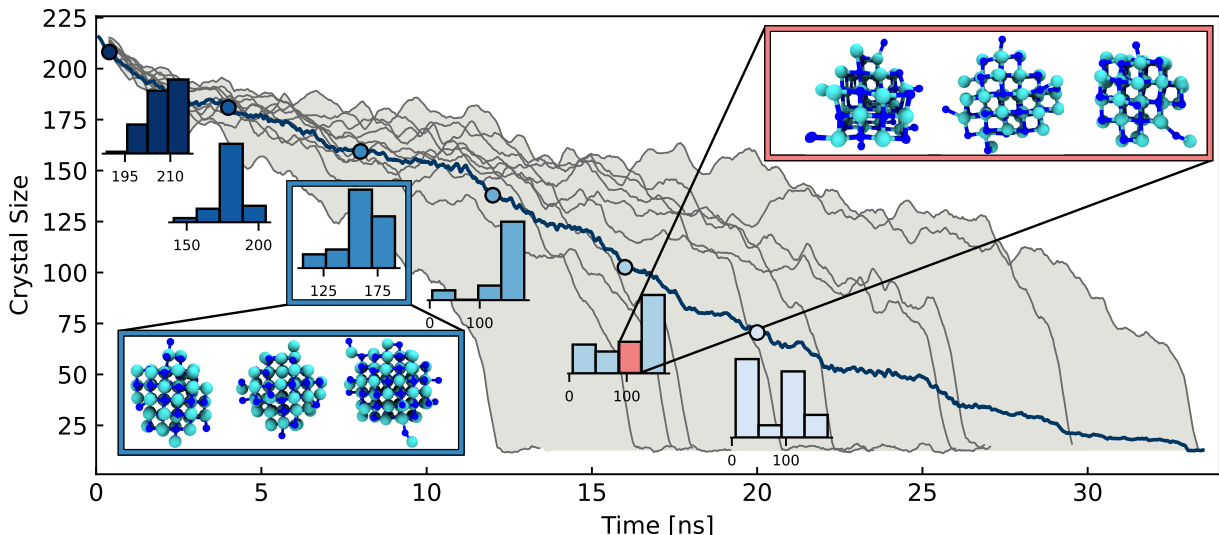


FIG. 3. **Overview of the stochastic nature of the NaCl dissolution process.** The main panel shows the crystal size over time for 10 simulations at 330 K initialised with random velocities for a $6 \times 6 \times 6$ nanocrystal. The range of fastest and slowest dissolving crystals is shaded in grey. The histograms show the distribution of crystal sizes across all trajectories for a given time window plotted along the mean crystal size (dark blue). Snapshots of crystals at 7 ns and with 87 ions are shown in the blue and red boxes respectively.

lution have limited their focus to individual trajectories, thus restricting the conclusions that can be drawn regarding the mechanism in this respect. However in this work, access to multiple *ab initio* quality trajectories via machine learning based simulations has enabled this issue to be addressed through a thorough statistical analysis over multiple trajectories.

Figure 3 shows the time evolution of the crystal size distribution for 10 trajectories of a $6 \times 6 \times 6$ nanocrystal. The size distribution is initially very narrow at the beginning of the dissolution. However as dissolution proceeds along the 10 trajectories, the distribution widens significantly. After approximately 15 ns, there is a spread of over 100 ions in the crystal sizes along different trajectories. While all trajectories follow the overall crumbling mechanism described in Section II, this broadening of the distributions illustrates the diverse microscopic paths taken by the crystals *en route* to dissolution. We previously discussed in Section II the highly dynamic equilibrium of microscopic subprocesses such as ions rolling on the crystal surface and lattice rearrangement occurring during the steady period of ion dissolution from the crystal. These are rooted in inherent stochastic system fluctuations such as lattice and molecular vibrations (on the order of fs) and water dipole and hydrogen bond reorientations (on the order of ps). Therefore the wide variation in the crystal structures at a given time (despite all simulations starting from the same pristine crystal structure) can be directly attributed to the stochastic nature of these microscopic sub-processes. Given the relatively small sizes of the systems studied here, one would expect a much larger spread of times in macroscopic systems. In

addition to the range of crystal sizes for different trajectories at a given time, for a given crystal size, there are also numerous possible structures, as shown in the inset of Figure 3, with 3 representative examples of a crystal with 87 atoms.

These diverse structures again arise from a combination of the stochastic microscopic subprocesses. The diversity in microscopic mechanism can also be observed for the other concentration conditions studied here. The largest $6 \times 6 \times 6$ crystal (5.61 mol/kg) takes much longer to dissolve and has a much broader range of dissolution times than the $4 \times 4 \times 4$ crystals (1.42 mol/kg and 2.84 mol/kg), as shown in Figure S10. This broad spread of times can be attributed to an increase in probability of ions rejoining the $6 \times 6 \times 6$ crystal, since it is surrounded by the lowest volume of water, but also there is a cumulative effect of each possible stochastic sub-process for every dissolution step. While a distribution of dissolution times is to be expected, a 2 or 3-fold spread in times is particularly noteworthy. In summary, the dissolution of NaCl therefore proceeds via an overall crumbling mechanism, within which, there is rich structural variety of the dissolving crystal owing to the inherently stochastic microscopic system fluctuations.

IV. CONCLUSION

Despite dissolution being one of the most ubiquitous processes on earth, major gaps in understanding at the atomistic level persist. In this work we provide a rigorous description of the mechanism of NaCl dissolution,

through the application of an automated framework to develop accurate MLPs. Surpassing the extent of previous simulation work we have generated multiple trajectories (> 300 ns in total) with *ab initio* equivalent accuracy, under a range of conditions of NaCl dissolving. We have established a general crumbling mechanism of NaCl dissolution, where following a steady period of ion-by-ion loss, the crystal reaches a critical point of instability and collapses in a concerted fashion. The sequence of dissolving ions in the steady period of dissolution is such that the number of ionic bonds broken and net charge on the crystalline lattice is minimised. The overall stability of a crystalline cluster in water can be straightforwardly reasoned by a delicate balance of interactions between the ions and water, measured via the surface area to volume ratio of the crystal. This simple and physically intuitive concept applies to NaCl and to other ionic crystals in water and can readily be extended to non-ionic systems such as molecular crystals. The crumbling mechanistic insights we have provided are primed for experimental measurement, including confinement controlled monitoring of the dissolution and Bragg coherent diffraction imaging, as have already been successfully applied to crystalline systems [12, 13].

We have shown that the overall nature of the dissolution mechanism is highly stochastic, comprising a dynamic equilibrium of sub-processes such as ions rolling, dissolving, rejoining and deformations of the lattice in the crystal. These arise from the stochastic hydrogen bond formation/breaking and thermal vibrations in the crystal and influence the relative stability of the crystal, and therefore the overall time taken for dissolution.

Given the sizes of the nanocrystals studied here, one could envisage a much larger spread of times in macroscopic systems such as those considered in the geosciences. Indeed, studies of dissolution of crystalline and non-crystalline materials in the earth sciences have observed a broad variation in the rate constant of dissolution of up to 2-3 orders of magnitude. [29, 55] which they attributed to the inhomogeneity of the initial crystal surface. However our results suggest that this variance in rate is inherent to the system, regardless of initial condition.

Such observations regarding the dynamic nature of the crystal are indeed very amenable to further experimental studies. They suggest a large variation in dissolution mechanism under flow compared to confinement. In the former case the ions are rapidly removed from the surface - similar to the lower ion concentration conditions we have shown here, while confinement essentially traps the ions, creating a high concentration of ions in the vicinity of the surface. We propose that revisiting the microfluidics [12] and electron microscopy [13] experiments described in the Introduction, with a focus on different concentration conditions would be highly insightful.

The accurate treatment of the electronic structure of the system required to capture relevant interactions, yet at a computational cost that facilitates the simulation of

many dissolution trajectories is crucial for the observations made here. The high transferability of the methodology and validation process is amenable to the study of other ionic salt systems. Indeed, having now understood NaCl dissolution – in terms of a minimization of charge and of bonds broken, a balance of ion-solvent interactions determining crystal stability, and the dynamic nature of the dissolution process – our work sets the stage for a generalised theory of dissolution of ionic crystals. Computing the solubility of the ML model is also an important next step, given the large differences from experiment in solubilities predicted by different force field models [54]. Finally, this methodology and the insights we have now obtained are primed for application to more challenging and complex systems of recent interest, including highly concentrated electrolyte solutions [56, 57] and electrolyte solutions under confinement [58].

V. METHODS

Machine Learning Potential: Machine learning potentials provide a direct functional relationship between atomic positions and forces/potential energy. This bypasses the otherwise computationally expensive requirement to solve Schrödinger-like equations and systems of much larger length and timescales than feasible with AIMD based approaches are now accessible. Building upon the seminal work of Behler and Parrinello in neural network based ML potentials [59], the recent development of an active learning approach using a committee of NNPs has enabled the systematic development and validation of NNP representations of the potential energy surface for complex aqueous systems [37, 60]

Our model was iteratively trained on forces and energies from carefully chosen *ab initio* molecular dynamics simulations in the generalised gradient approximation using the rev-PBE functional with Grimme’s D3 dispersion correction [61], while using a Coulomb baseline to incorporate the correct long-range electrostatics, evaluated with particle mesh Ewald summation. This baseline uses TIP3P model parameters [62] for water and point charges of ± 1 for Na and Cl. This setup has been shown to be accurate for aqueous systems, and further details on functional selection and long-range electrostatics are described in the SI.

The model was iteratively improved over multiple generations such that the relevant configuration space was accurately covered in the overall training set with an energy and force root mean square error (RMSE) of 1.3 meV per atom and 38.0 meV/Å, respectively. The model was extensively validated in a series of tests incorporating static and dynamical properties of selected test systems of which full details are also given in the SI.

MD simulations: The systems used in all dissolution simulations described comprised a $4 \times 4 \times 4$ ($6 \times 6 \times 6$) NaCl nanocrystal with 32 (108) Na/Cl atoms using a computed lattice constant of 5.72 Å [63]. The $4 \times 4 \times 4$ nanocrystal

was surrounded by 625 (1250) water molecules in a cubic simulation cell of side length 27.8 Å (34.1 Å), giving dissolved NaCl concentrations in water of 2.84 mol/kg and 1.43 mol/kg respectively. The $6 \times 6 \times 6$ crystal was surrounded by 1068 waters in a cubic simulation cell of side length 34.1 Å giving a dissolved NaCl concentration in water of 5.61 mol/kg. MLP simulations were all carried out using the CP2K/Quickstep code in the NVT ensemble and at a constant temperature of 330 K (chosen to be consistent with previous literature [64]) maintained using the CSV thermostat [65]. At each concentration, 10 trajectories were simulated using the same initial configuration and initialised with random velocities drawn from the Boltzmann distribution at the target temperature of 330 K. Simulations were run for over 15 ns (5.61 mol/kg), 2 ns (2.84 mol/kg) and 1 ns (1.42 mol/kg) until the crystal was fully dissolved. The same simulation procedure was carried out for 10 trajectories of the 2.42 mol/kg concentration at 400 K for further validation of the generalisability of our conclusions. These results are included in the SI. Overall over 300 ns of *ab initio* quality machine learning based simulations were performed, far beyond the capabilities of AIMD simulations.

Further details for computing parameters including cluster size, \bar{q}_8 and surface area to volume ratio of the crystal are given in the SI.

VI. ACKNOWLEDGMENTS

We are grateful to Daan Frenkel for helpful discussions. We thank Julian Gale for his insightful comments on the manuscript. N.O.N acknowledges financial support from the Gates Cambridge Trust. C.S acknowledges financial support from the Alexander von Humboldt Stiftung. S.J.C is a Royal Society University Research Fellow (URF\R 1\211144) at the University of Cambridge. We are grateful for computational support and resources from the UK Materials and Molecular Modeling Hub which is partially funded by EPSRC (Grant Nos. EP/P020194/1 and EP/T022213/1). We are also grateful for computational support and resources from the UK national high-performance computing service, Advanced Research Computing High End Resource (ARCHER2). Access for both the UK Materials and Molecular Modeling Hub and ARCHER2 were obtained via the UK Car-Parrinello consortium, funded by EPSRC grant reference EP/P022561/1.

REFERENCES

-
- [1] Liumin Suo, Yong Sheng Hu, Hong Li, Michel Armand, and Liqian Chen, “A new class of Solvent-in-Salt electrolyte for high-energy rechargeable metallic lithium batteries,” *Nat. Commun.* **4**, 1481 (2013).
 - [2] Menachem Elimelech and William A. Phillip, “The future of seawater desalination: Energy, technology, and the environment,” *Science*. **333**, 712–717 (2011).
 - [3] Gordon L. Amidon, Hans Lennernäs, Vinod P. Shah, and John R. Crison, “A Theoretical Basis for a Biopharmaceutical Drug Classification: The Correlation of in Vitro Drug Product Dissolution and in Vivo Bioavailability,” *Pharm. Res.* **12**, 413–420 (1995).
 - [4] Jillian F. Banfield, William W. Barker, Susan A. Welch, and Anne Taunton, “Biological impact on mineral dissolution: Application of the lichen model to understanding mineral weathering in the rhizosphere,” *Proc. Natl. Acad. Sci. U. S. A.* **96**, 3404–3411 (1999).
 - [5] Kenneth S. Pitzer, J. Christopher Peiper, and R. H. Busey, “Thermodynamic Properties of Aqueous Sodium Chloride Solutions,” *J. Phys. Chem. Ref. Data* **13**, 1–102 (1984).
 - [6] Gabriele C. Sosso, Ji Chen, Stephen J. Cox, Martin Fitzner, Philipp Pedevilla, Andrea Zen, and Angelos Michaelides, “Crystal Nucleation in Liquids: Open Questions and Future Challenges in Molecular Dynamics Simulations,” *Chem. Rev.* **116**, 7078–7116 (2016).
 - [7] G. Wulff, “XXV. Zur Frage der Geschwindigkeit des Wachstums und der Auflösung der Krystallflächen,” *Zeitschrift für Krist. - Cryst. Mater.* **34**, 449–530 (1901).
 - [8] L. Xu, H. Bluhm, and M. Salmeron, “An AFM study of the tribological properties of NaCl (100) surfaces under moist air,” *Surf. Sci.* **407**, 251–255 (1998).
 - [9] Jinbo Peng, Jing Guo, Runze Ma, Xiangzhi Meng, and Ying Jiang, “Atomic-scale imaging of the dissolution of NaCl islands by water at low temperature,” *J. Phys. Condens. Matter* **29**, 104001 (2017).
 - [10] Jesse N. Clark, Johannes Ihli, Anna S. Schenk, Yi Yeoun Kim, Alexander N. Kulak, James M. Campbell, Gareth Nisbet, Fiona C. Meldrum, and Ian K. Robinson, “Three-dimensional imaging of dislocation propagation during crystal growth and dissolution,” *Nat. Mater.* **14**, 780–784 (2015).
 - [11] Qiubo Zhang, Xinxing Peng, Yifan Nie, Qi Zheng, Junyi Shangguan, Chao Zhu, Karen C. Bustillo, Peter Ercius, Linwang Wang, David T. Limmer, and Haimei Zheng, “Defect-mediated ripening of core-shell nanostructures,” *Nat. Commun.* **13**, 2211 (2022).
 - [12] Dan Lis, Ellen H.G. Backus, Johannes Hunger, Sapun H. Parekh, and Mischa Bonn, “Liquid flow along a solid surface reversibly alters interfacial chemistry,” *Science*. **344**, 1138–1142 (2014).
 - [13] Takayuki Nakamuro, Masaya Sakakibara, Hiroki Nada, Koji Harano, and Eiichi Nakamura, “Capturing the Moment of Emergence of Crystal Nucleus from Disorder,” *J. Am. Chem. Soc.* **143**, 1763–1767 (2021).
 - [14] Jihan Zhou, Yongsoo Yang, Yao Yang, Dennis S. Kim, Andrew Yuan, Xuezheng Tian, Colin Ophus, Fan Sun, Andreas K. Schmid, Michael Nathanson, Hendrik Heinz, Qi An, Hao Zeng, Peter Ercius, and Jianwei Miao, “Observing crystal nucleation in four dimensions using atomic electron tomography,” *Nature* **570**, 500–503 (2019).

- [15] Alessandro Silvestri, Paolo Raiteri, and Julian D. Gale, "Obtaining Consistent Free Energies for Ion Binding at Surfaces from Solution: Pathways versus Alchemy for Determining Kink Site Stability," *J. Chem. Theory Comput.* **18**, 5901–5919 (2022).
- [16] J. L. Aragoñes, E. Sanz, and C. Vega, "Solubility of NaCl in water by molecular simulation revisited," *J. Chem. Phys.* **136**, 244508 (2012).
- [17] Inna Kurganskaya and Andreas Luttmann, "Kinetic monte carlo simulations of silicate dissolution: Model complexity and parametrization," *J. Phys. Chem. C* **117**, 24894–24906 (2013).
- [18] Jian-Cheng Chen, Bernhard Reischl, Peter Spijker, Nico Holmberg, Kari Laasonen, and Adam S Foster, "Ab initio Kinetic Monte Carlo simulations of dissolution at the NaCl–water interface," *Phys. Chem. Chem. Phys.* **16**, 22545–22554 (2014).
- [19] Maximilian Greiner, Ekaterina Elts, and Heiko Briesen, "Insights into pharmaceutical nanocrystal dissolution: A molecular dynamics simulation study on aspirin," *Mol. Pharm.* **11**, 3009–3016 (2014).
- [20] C. André Ohlin, Eric M. Villa, James R. Rustad, and William H. Casey, "Dissolution of insulating oxide materials at the molecular scale," *Nat. Mater.* **9**, 11–19 (2010).
- [21] J. H. Harding and S. C. Parker, "Molecular dynamics simulation of crystal dissolution from calcite steps," *Phys. Rev. B* **60**, 13792 (1999).
- [22] Patricia M. Dove, Nizhou Han, and James J. De Yoreo, "Mechanisms of classical crystal growth theory explain quartz and silicate dissolution behavior," *Proc. Natl. Acad. Sci. U. S. A.* **102**, 15357–15362 (2005).
- [23] Amy E. Hofmann, Ian C. Bourg, and Donald J. DePaolo, "Ion desolvation as a mechanism for kinetic isotope fractionation in aqueous systems," *Proc. Natl. Acad. Sci. U. S. A.* **109**, 18689–18694 (2012).
- [24] Marco De La Pierre, Paolo Raiteri, Andrew G. Stack, and Julian D. Gale, "Uncovering the Atomistic Mechanism for Calcite Step Growth," *Angew. Chemie - Int. Ed.* **56**, 8464–8467 (2017).
- [25] Stefano Piana and Julian D. Gale, "Understanding the barriers to crystal growth: Dynamical simulation of the dissolution and growth of urea from aqueous solution," *J. Am. Chem. Soc.* **127**, 1975–1982 (2005).
- [26] Yunjian Li, Hui Pan, Qing Liu, Xing Ming, and Zongjin Li, "Ab initio mechanism revealing for tricalcium silicate dissolution," *Nat. Commun.* **13**, 1253 (2022).
- [27] Yi Gao and Kenneth W. Olsen, "Molecular dynamics of drug crystal dissolution: Simulation of acetaminophen form I in water," *Mol. Pharm.* **10**, 905–917 (2013).
- [28] Patricia M. Dove and Nizhou Han, "Kinetics of Mineral Dissolution and Growth as Reciprocal Microscopic Surface Processes Across Chemical Driving Force," *AIP Conf. Proc.* **916**, 215 (2007).
- [29] Cornelius Fischer, Rolf S. Arvidson, and Andreas Luttmann, "How predictable are dissolution rates of crystalline material?" *Geochim. Cosmochim. Acta* **98**, 177–185 (2012).
- [30] Hao Jiang, Pablo G. Debenedetti, and Athanassios Z. Panagiotopoulos, "Nucleation in aqueous NaCl solutions shifts from 1-step to 2-step mechanism on crossing the spinodal," *J. Chem. Phys.* **150**, 124502 (2019).
- [31] Aaron R. Finney and Matteo Salvalaglio, "Multiple pathways in NaCl homogeneous crystal nucleation," *Faraday Discuss.* **235**, 56–80 (2021).
- [32] C. P. Lamas, J. R. Espinosa, M. M. Conde, J. Ramírez, P. Montero De Híjes, E. G. Noya, C. Vega, and E. Sanz, "Homogeneous nucleation of NaCl in supersaturated solutions," *Phys. Chem. Chem. Phys.* **23**, 26843–26852 (2021).
- [33] Pei Lin Kang, Cheng Shang, and Zhi Pan Liu, "Large-Scale Atomic Simulation via Machine Learning Potentials Constructed by Global Potential Energy Surface Exploration," *Acc. Chem. Res.* **53**, 2119–2129 (2020).
- [34] Volker L. Deringer, Miguel A. Caro, and Gábor Csányi, "Machine Learning Interatomic Potentials as Emerging Tools for Materials Science," *Adv. Mater.* **31**, 1902765 (2019).
- [35] Jörg Behler, "Perspective: Machine learning potentials for atomistic simulations," *J. Chem. Phys.* **145**, 170901 (2016).
- [36] Jörg Behler, "Four Generations of High-Dimensional Neural Network Potentials," *Chem. Rev.* **121**, 10037–10072 (2021).
- [37] Christoph Schran, Fabian L. Thiemann, Patrick Rowe, Erich A. Müller, Ondrej Marsalek, and Angelos Michaelides, "Machine learning potentials for complex aqueous systems made simple," *Proc. Natl. Acad. Sci. U. S. A.* **118**, 38 (2021).
- [38] Gabriele Lanaro and G. N. Patey, "Molecular dynamics simulation of NaCl dissolution," *J. Phys. Chem. B* **119**, 4275–4283 (2015).
- [39] Jiří Klimeš, David R. Bowler, and Angelos Michaelides, "Understanding the role of ions and water molecules in the NaCl dissolution process," *J. Chem. Phys.* **139**, 234702 (2013).
- [40] Li-Min Liu, Alessandro Laio, and Angelos Michaelides, "Initial stages of salt crystal dissolution determined with ab initio molecular dynamics," *Phys. Chem. Chem. Phys.* **13**, 13162–13166 (2011).
- [41] Nico Holmberg, Jian-Cheng Chen, Adam S Foster, and Kari Laasonen, "Dissolution of NaCl nanocrystals: an ab initio molecular dynamics study," *Phys. Chem. Chem. Phys.* **16**, 17437–17446 (2014).
- [42] Alex P. Gaiduk and Giulia Galli, "Local and Global Effects of Dissolved Sodium Chloride on the Structure of Water," *J. Phys. Chem. Lett.* **8**, 1496–1502 (2017).
- [43] Cunzhi Zhang, Federico Giberti, Emre Sevgen, Juan J. de Pablo, Francois Gygi, and Giulia Galli, "Dissociation of salts in water under pressure," *Nat. Commun.* **11**, 3037 (2020).
- [44] Mark N. Joswiak, Michael F. Doherty, and Baron Peters, "Ion dissolution mechanism and kinetics at kink sites on NaCl surfaces," *Proc. Natl. Acad. Sci. U. S. A.* **115**, 656–661 (2018).
- [45] Kazuya Kobayashi, Yunfeng Liang, Tetsuo Sakka, and Toshifumi Matsuoka, "Molecular dynamics study of salt–solution interface: Solubility and surface charge of salt in water," *J. Chem. Phys.* **140**, 144705 (2014).
- [46] V. Bianco, M. M. Conde, C. P. Lamas, E. G. Noya, and E. Sanz, "Phase diagram of the NaCl–water system from computer simulations," *J. Chem. Phys.* **156**, 064505 (2022).
- [47] Yong Yang, Sheng Meng, L F Xu, E G Wang, and Shiwu Gao, "Dissolution dynamics of NaCl nanocrystal in liquid water," *Phys. Rev. E* **72**, 12602 (2005).
- [48] Chunyi Zhang, Shuwen Yue, Athanassios Z. Panagiotopoulos, Michael L. Klein, and Xifan Wu, "Dissolving salt is not equivalent to applying a pressure on wa-

- ter,” *Nat. Commun.* **13**, 822 (2022).
- [49] Timothy J. Flowers, Rana Munns, and Timothy D. Colmer, “Sodium chloride toxicity and the cellular basis of salt tolerance in halophytes,” *Ann. Bot.* **115**, 419–431 (2015).
- [50] W. R. Simpson, R. Von Glasow, K. Riedel, P. Anderson, P. Ariya, J. Bottenheim, J. Burrows, L. J. Carpenter, U. Frieß, M. E. Goodsite, D. Heard, M. Hutterli, H. W. Jacobi, L. Kaleschke, B. Neff, J. Plane, U. Platt, A. Richter, H. Roscoe, R. Sander, P. Shepson, J. Sodeau, A. Steffen, T. Wagner, and E. Wolff, “Halogens and their role in polar boundary-layer ozone depletion,” *Atmos. Chem. Phys.* **7**, 4375–4418 (2007).
- [51] B. J. Finlayson-Pitts, “The Tropospheric Chemistry of Sea Salt: A Molecular-Level View of the Chemistry of NaCl and NaBr,” *Chem. Rev.* **103**, 4801–4822 (2003).
- [52] Kevin Leung, “First-Principles Modeling of Mn(II) Migration above and Dissolution from LixMn₂O₄ (001) Surfaces,” *Chem. Mater.* **29**, 2550–2562 (2017).
- [53] Ei Hayakawaf, Nobuhiro Fukushima, Isao Okada, and Ei Hayakawaf, “Dissolution Process of Sodium Chloride Crystal in Water,” *Pure Appl. Chem.* **60**, 1321–1324 (1988).
- [54] A. L. Benavides, J. L. Aragonés, and C. Vega, “Consensus on the solubility of NaCl in water from computer simulations using the chemical potential route,” *The Journal of Chemical Physics* **144**, 124504 (2016).
- [55] Inna Kurganskaya and Andreas Luttmge, “Mineral Dissolution Kinetics: Pathways to Equilibrium,” *ACS Earth Sp. Chem.* **5**, 1657–1673 (2021).
- [56] Timothy S. Groves, Carla S. Perez-Martinez, Romain Lhermerout, and Susan Perkin, “Surface Forces and Structure in a Water-in-Salt Electrolyte,” *J. Phys. Chem. Lett.* **12**, 1702–1707 (2021).
- [57] Alexander M. Smith, Alpha A. Lee, and Susan Perkin, “The Electrostatic Screening Length in Concentrated Electrolytes Increases with Concentration,” *J. Phys. Chem. Lett.* **7**, 2157–2163 (2016).
- [58] Wenhui Zhao, Yunxiang Sun, Weiduo Zhu, Jian Jiang, Xiaorong Zhao, Dongdong Lin, Wenwu Xu, Xiangmei Duan, Joseph S. Francisco, and Xiao Cheng Zeng, “Two-dimensional monolayer salt nanostructures can spontaneously aggregate rather than dissolve in dilute aqueous solutions,” *Nat. Commun.* **12**, 5602 (2021).
- [59] Jörg Behler and Michele Parrinello, “Generalized neural-network representation of high-dimensional potential-energy surfaces,” *Phys. Rev. Lett.* **98**, 146401 (2007).
- [60] Christoph Schran, Krystof Brezina, and Ondrej Marsalek, “Committee neural network potentials control generalization errors and enable active learning,” *J. Chem. Phys.* **153**, 104105 (2020).
- [61] Stefan Grimme, Jens Antony, Stephan Ehrlich, and Helge Krieg, “A consistent and accurate ab initio parametrization of density functional dispersion correction (DFT-D) for the 94 elements H-Pu,” *J. Chem. Phys.* **132**, 154104 (2010).
- [62] William L Jorgensen, Jayaraman Chandrasekhar, Jeffrey D Madura, Roger W Impey, and Michael L Klein, “Comparison of simple potential functions for simulating liquid water,” *J. Chem. Phys.* **79**, 926–935 (1983).
- [63] Li-Min Liu, Matthias Krack, and Angelos Michaelides, “Interfacial water: A first principles molecular dynamics study of a nanoscale water film on salt,” *J. Chem. Phys.* **130**, 234702 (2009).
- [64] Li-Min Liu, Matthias Krack, and Angelos Michaelides, “Density Oscillations in a Nanoscale Water Film on Salt: Insight from Ab Initio Molecular Dynamics,” *J. Am. Chem. Soc.* **130**, 8572–8573 (2008).
- [65] Giovanni Bussi, Davide Donadio, and Michele Parrinello, “Canonical sampling through velocity rescaling,” *J. Chem. Phys.* **126**, 14101 (2007).

Supporting Information for: Crumbling Crystals: On the Dissolution Mechanism of NaCl in Water

Niamh O'Neill,¹ Christoph Schran,^{1,2, a)} Stephen J. Cox,¹ and Angelos Michaelides^{1,2, b)}

¹⁾ *Yusuf Hamied Department of Chemistry, University of Cambridge, Lensfield Road, Cambridge, CB2 1EW, UK*

²⁾ *Thomas Young Centre, London Centre for Nanotechnology, and Department of Physics and Astronomy, University College London, Gower Street, London, WC1E 6BT, United Kingdom*

^{a)}Electronic mail: cs2121@cam.ac.uk

^{b)}Electronic mail: am452@cam.ac.uk

CONTENTS

S1. Selecting DFT functional	S2
S2. Development of Machine Learning Potential	S5
Automated Work Flow	S5
Details of Model	S6
Validation	S9
$2 \times 2 \times 2$ NaCl nanocrystal	S9
Validation of Dissolution Process	S10
Long-range Effects	S12
S3. Molecular dynamics simulations	S14
System setups	S14
Simulation details	S15
Force field pre-equilibration details	S16
AIMD simulation details	S17
S4. Analysis Details	S17
Steinhardt order parameters	S17
Coordination Numbers and clusters	S18
S5. Additional Results	S20
MLP	S20
FF	S20
References	S21
References	S21

S1. SELECTING DFT FUNCTIONAL

Two modern DFT functionals that have been shown to perform well for liquid water simulations^{S1,S2} - the dispersion corrected GGA functional revPBE-D3^{S3,S4} and the strongly constrained and appropriately normed (SCAN) meta-GGA functional^{S5}- were selected for

an initial benchmark study to determine the most suitable XC functional for the *ab initio* simulations upon which the MLP would be trained. It should be noted that dispersion corrected hybrid functionals have been shown to provide slightly better results for liquid water simulations;^{S6,S7} however initial simulations with revPBE0-D3 showed there is approximately a six-fold increase in computational cost, rendering longer time-scale AIMD simulations unfeasible for the envisaged system sizes.

Na/Cl ion in water

To study the performance of SCAN and revPBE-D3 for ion-water simulations, four separate AIMD simulations were performed for both revPBE-D3 and SCAN for Na⁺ in water and Cl⁻ in water. The Na(Cl)-O RDF $g(r)$ are compared to experimental values in Figure S1 and Table I. Both SCAN and revPBE-D3 are in good agreement with the position of the first experimental Cl-O peak (R_{\max}^1), where both are within 0.07 Å of the experimental data. However the height $g(R_{\max}^1)$ is underestimated by both by approximately 15%. SCAN and revPBE-D3 both qualitatively agree with the position of the second peak maximum, but they both tend to overstructure compared to experiment. The experimental Na-O peak is more accurately reproduced by SCAN than revPBE-D3. The revPBE-D3 peak is shifted 0.17 Å from the experimental value, and the peak height is 27% lower. This is also in agreement with previous studies, where SCAN has been shown to outperform GGA functionals in reproducing the sodium-water solvation structure.^{S8} Despite a lack of experimental data for the second solvation shell, revPBE-D3 is in much closer qualitative agreement with SCAN than for the first peak.

TABLE I. Summary of structural properties of solvated sodium/chloride ions obtained from RDFs $g(r)$ computed from AIMD simulations with SCAN and revPBE-D3 at 300 K. Experimental reference data for Cl-O and Na-O were obtained from neutron diffraction^{S9} and X-Ray diffraction^{S2} data respectively. Difference from experiment is shown in brackets.

	Cl-O			Na-O		
	SCAN	revPBE-D3	Experiment	SCAN	revPBE-D3	Experiment
R_{\max}^1 (Å)	3.10 (0.07)	3.19 (0.02)	3.17	2.36 (0.00)	2.53 (0.17)	2.36
$g(R_{\max}^1)$	2.83 (0.62)	2.70 (0.51)	3.21	5.79 (0.08)	4.30 (0.43)	5.87

The O-O RDF for both solvated sodium and chloride ion systems was also computed and compared to experiment in order to evaluate the performance of the two functionals

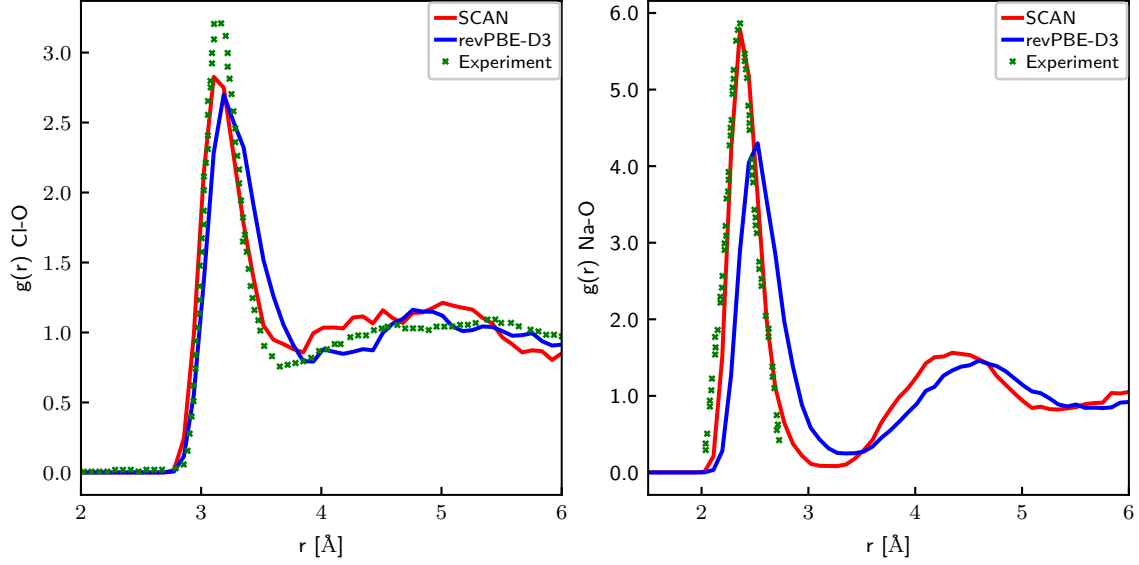


FIG. S1. Radial distribution function $g(r)$ for Cl-O (left) and Na-O (right) comparing revPBE-D3 and SCAN with experiment. Cl-O experimental RDF obtained from neutron diffraction data^{S9} and Na-O experimental RDF obtained from X-Ray diffraction data.^{S8}

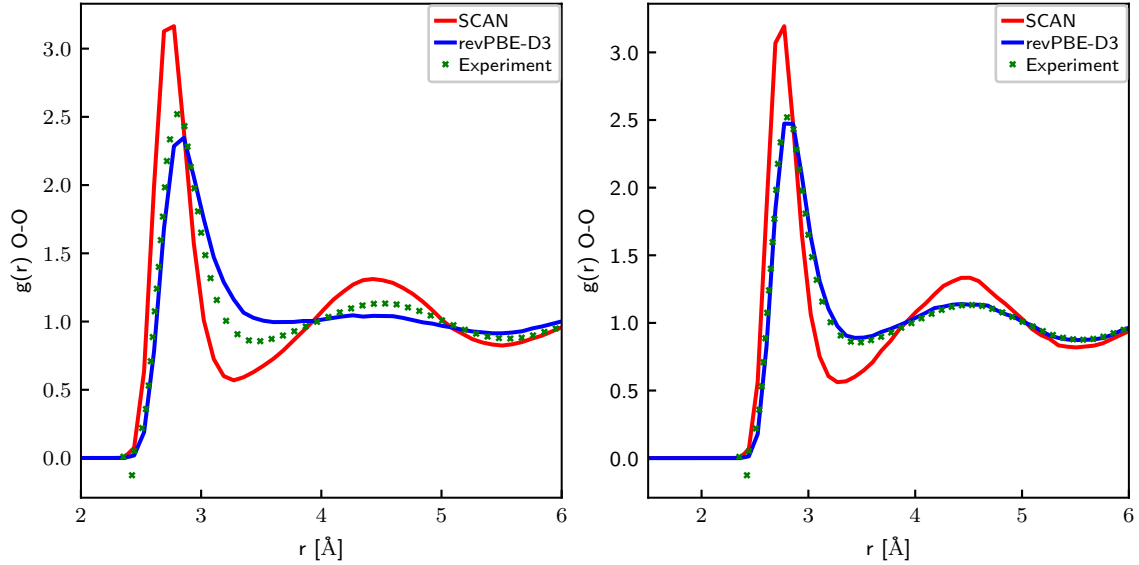


FIG. S2. Radial distribution function $g(r)$ for O-O for $\text{Cl}^-/\text{H}_2\text{O}$ (left) and $\text{Na}^+/\text{H}_2\text{O}$ (right). Compared to experimental data taken from Ref. S10.

for water. This analysis is shown below in Figure S2. In both cases, SCAN significantly overstructures water compared to revPBE-D3 and experiment, with a first peak maximum approximately 25% greater than experiment. This is consistent with literature results, in which Duignan et al. compared the performance of revPBE-D3 and SCAN in simulations of liquid water at 300 K.^{S8} revPBE-D3 reproduced well the experimental O-O radial distri-

bution function (RDF), with the first peak maximum and magnitude coinciding to within 0.1 Å and 2% respectively, while SCAN overstructured water, with a first peak RDF maximum approximately 20% larger than experiment. Galib et al. also report a computed water density with revPBE-D3 of $0.962 \pm 0.029 \text{ gcm}^{-3}$ within 4% of the experimental density of 0.997 gcm^{-3} ,^{S2} compared to a computed density by Wiktor et al. of 1.05 gcm^{-3} .^{S11}

In summary, the decision between SCAN and revPBE-D3 is not completely clear-cut and both functionals have advantages and disadvantages. revPBE-D3 performs better for liquid water than SCAN. With respect to the solvated ions, revPBE-D3 is on par with SCAN for the Cl-O interactions, however performs significantly poorer for Na-O. Nevertheless, revPBE-D3 reproduces experimental data much better than SCAN with respect to the O-O RDF. As a footnote, SCAN is also two-thirds more expensive than revPBE-D3. Therefore, the AIMD trajectories generated using revPBE-D3 were chosen for the initial development of the C-NNP training set and revPBE-D3 was used for generation of subsequent AIMD data and during the active learning stages of the MLP development.

S2. DEVELOPMENT OF MACHINE LEARNING POTENTIAL

Automated Work Flow

The procedure for developing the committee neural network potential (C-NNP) was followed as described in Ref S12. The general approach taken in developing the C-NNP was to treat different relevant systems and conditions individually with active learning, generating a training set for each condition and then combining the individual training sets to generate the final model. The model was iteratively improved over five generations of such active learning rounds, with each generation targeting a specific region of phase space. The overall development over these five generations of the model is summarised in Figure S3. An initial potential was trained on forces and energies obtained from *ab initio* simulations described in Section S3 comprising bulk water, individual Na^+ / Cl^- ions in water, an Na^+ / Cl^- ion pair in water and a small 2×2 nanocrystal in water. This model was then used under different temperatures to generate structures along the dissolution trajectory of the prototypical $4 \times 4 \times 4$ nanocrystal (Generation 2). Later generations of the model targeted solution and intermediate structures along the dissolution trajectory (Generations 3+4) and highly con-

centrated solutions (Generation 5). The development of the model used the Python AML active learning package described in Ref. S13. For a given active learning iteration, 20 random structures from a reference trajectory were used to initialise the model. After training 8 NNP members, forces and energies of 2000 randomly selected structures from the reference trajectory were predicted to ascertain the force and energy committee disagreements. 20 structures with the largest mean force disagreement were added to the training set for the next round of active learning. Convergence was reached when new structures added to the training set did not improve the committee disagreement between points already in the training set, indicating the training set was sufficiently diverse. The training set of the final C-NNP model contained 1608 structures. The overall force and energy training root mean square error (RMSE) for the model are 38.0 meV/Å and 1.3 meV/atom respectively. Given the complexity of the system under study, this compares well to a RMSE of 70 meV/Å quoted in Ref. S14 for a simpler system of large scale MD simulations of water using NNPs trained on DFT.

Details of Model

The chemical environment around each atom was described using a general set of atom-centered symmetry functions.^{S15} There are 10 radial and 4 angular functions for each pair and triple of atoms, following Ref. S12. All symmetry functions used a cutoff function of angular cosine form with a cutoff radius of 12 Bohr. The committee was comprised of 8 NNP members, of identical architecture with 2 hidden layers and 25 neurons in each layer. In all cases, random sub-sampling was performed to introduce variability between the committee members, where 10% of the total set of structures were discarded. The weights and biases of the NNPs were optimised using the n2p2 code.^{S16} Individual models during active learning were optimised for 15 epochs, while the final C-NNP model used in simulations was optimised for 50 epochs.

To ensure that long-range effects are accurately captured by the machine learning potential, we explicitly incorporated long-range effects beyond the cutoff of the symmetry functions (12 Bohr). The predicted energy can in general be written as a sum of short range and long range contributions (E_{sr} and E_{coul} respectively): $E_{tot} = E_{sr} + E_{coul}$. The long-range model was thus trained on the difference between the standard short-ranged model

and the Coulomb contribution, calculated using point charges of +/- 1 respectively for Na and Cl and using TIP3P model parameters for water.^{S17} We used this model in all production simulations, where the Coulomb contributions were explicitly included via particle mesh ewald summation. Details on the validation of the final model and the role of long range interactions in these simulations are presented in the next Section.

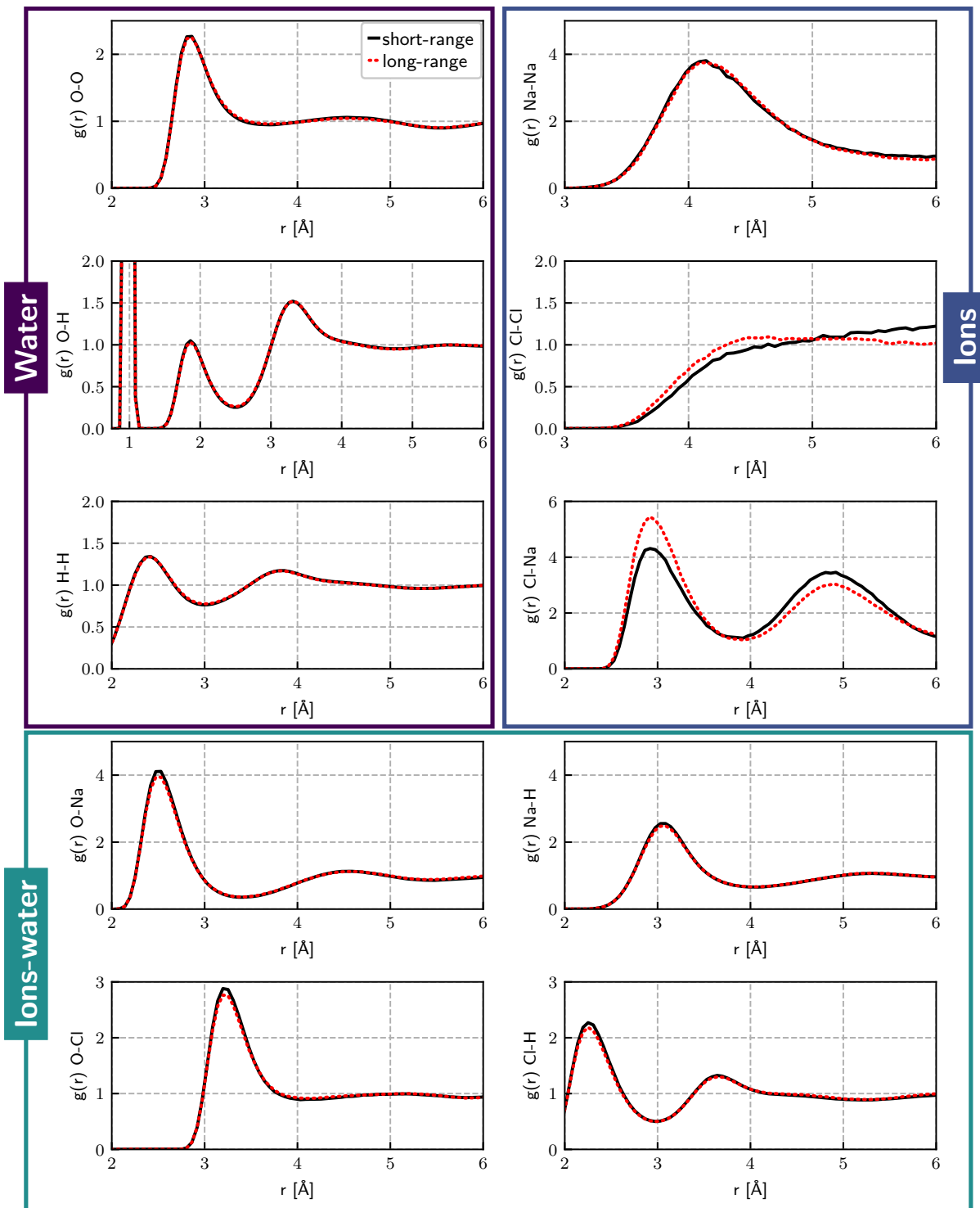


FIG. S3. Summary of iterative development of MLP over 5 generations. The number of configurations included from each AIMD simulation is given in Generation-01. Thereafter, the number of configurations is the total number of structures in the training set for the given generation.

Validation

The system studied is complex, so care was taken to set up a series of validation tests that incorporates relevant subsystems and properties.

$2 \times 2 \times 2$ *NaCl nanocrystal*

The static and dynamical properties of the largest accessible NaCl nanocrystal in water for AIMD simulations ($2 \times 2 \times 2$ NaCl surrounded by 229 waters - 695 atoms) was analysed using a benchmarking scheme proposed in Ref. S12, comparing AIMD to the C-NNP predictions and shown in Figure S4. The radial distribution functions (RDFs) $g(r)$ for all the atom species of the system gives a good assessment of the ability of the C-NNP to predict thermodynamic properties. The vibrational density of states (VDOS) for each element gives information on the vibrational modes of the system, and thus the dynamics of inter- and intra-atomic interactions. The forces on the atoms are sensitive to the local environment, and give additional insight via which the quality of the ML model can be evaluated. RDF and VDOS predictions are all in essentially perfect agreement with the AIMD reference trajectory while the force predictions and the DFT reference are very well correlated. It should be noted that the slight discrepancy in the VDOS between the C-NNP and AIMD at higher frequencies is likely due to the large plane wave cutoff required in the DFT calculations to obtain converged Na forces (Discussed in further detail in Section S3). Nevertheless the symmetry between Na and Cl VDOS spectra is reassuring.

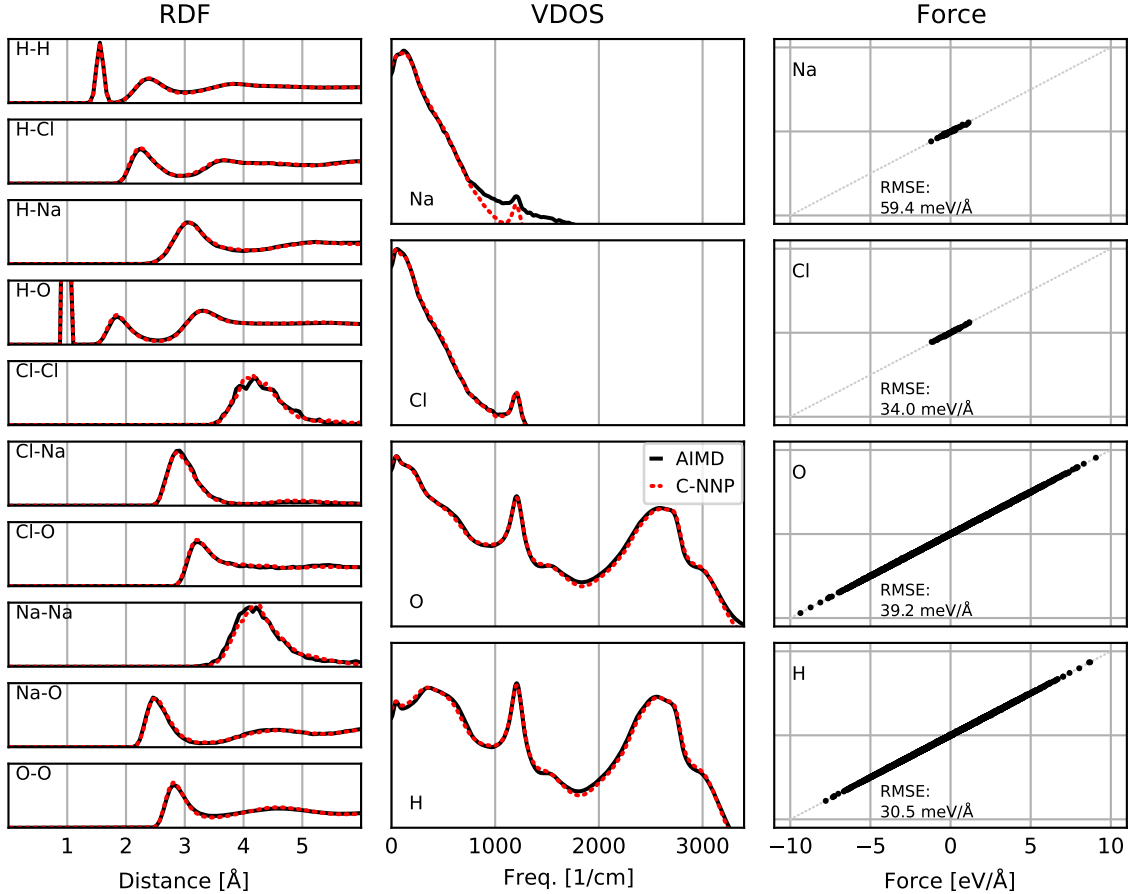


FIG. S4. Benchmark tests of long-range C-NNP model predictions of structural and dynamical properties of a $2 \times 2 \times 2$ NaCl nanocrystal in water as well as force prediction. The comparison between AIMD and the C-NNP RDFs, VDOS and force correlation are shown in the left, middle and right panels respectively.

Validation of Dissolution Process

As the most rigorous of tests for the C-NNP we validate the ML model for the actual dissolution process of a $4 \times 4 \times 4$ nanocrystal in solution by comparing the force and energy predictions of the model and the corresponding DFT forces and energies for a set of structures uniformly selected along the dissolution process. It is particularly valuable since the model has not been explicitly trained on these structures. First, an extensive MD simulation with the developed model was performed in order to sample the dissolution process of the $4 \times 4 \times 4$ nanocrystal in solution. A variety of structures were selected to capture all of the relevant configurations along the trajectory; from the intact NaCl crystal lattice, to the initial stages of dissolution to the end point of the fully solvated ions in solution. Next, the DFT reference

energies and forces of these 50 structures were computed. The resulting correlation of the forces is shown in Figure S5. The RMSE values for both forces ($37.0 \text{ meV}/\text{\AA}$) and energies ($0.3 \text{ meV}/\text{atom}$) compare very favourably to similar reactive systems, which have been studied using machine learning potentials, such as the work by Behler et al. in Ref. S18 who quote a force and energy RMSE for a model describing proton transport at ZnO/H₂O interfaces of $140.4 \text{ meV}/\text{\AA}$ and $1.0 \text{ meV}/\text{atom}$ respectively.

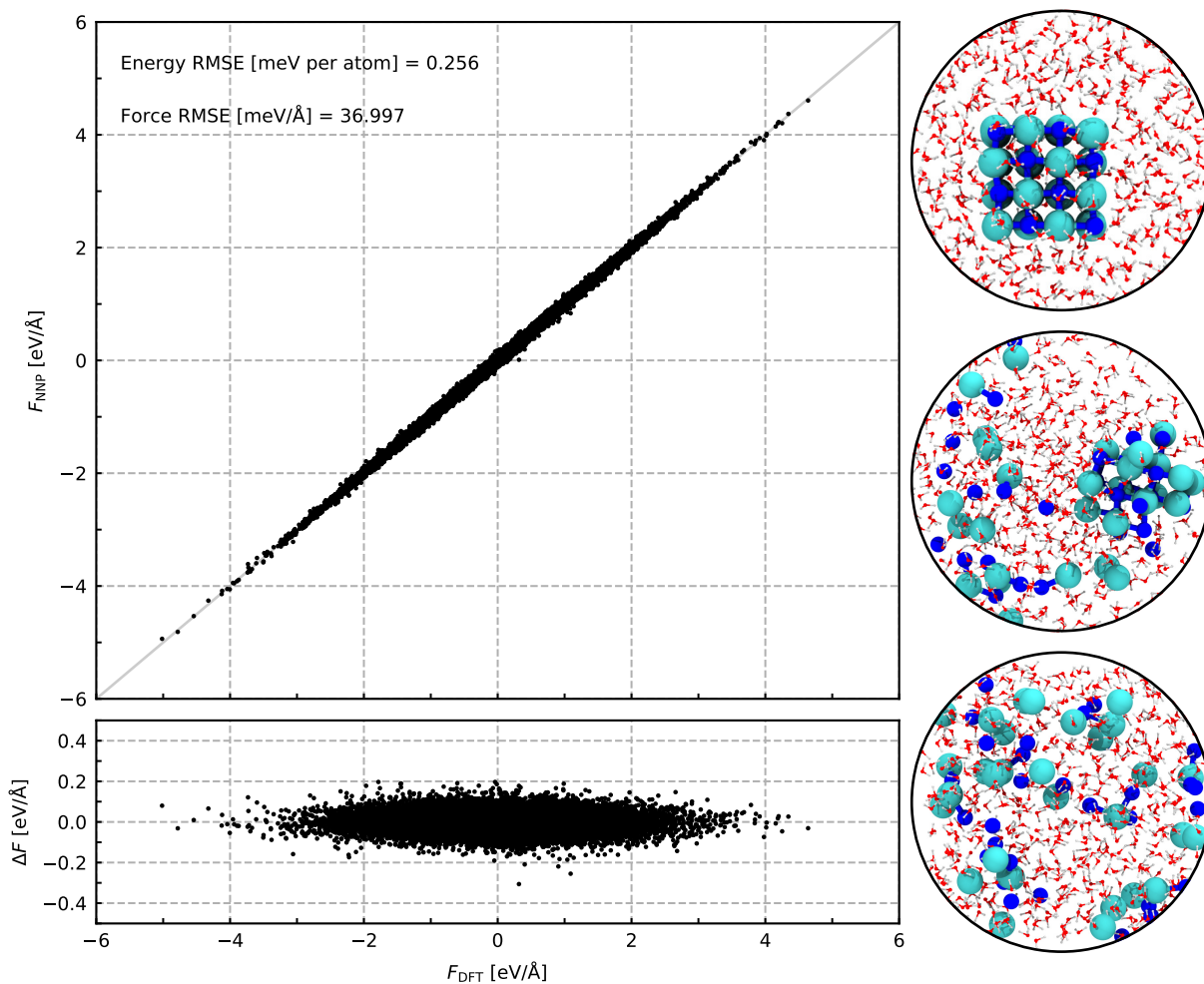


FIG. S5. Correlation plot for C-NNP predicted forces and corresponding reference DFT forces, with light grey line showing a perfect correlation coefficient of 1. Representative snapshots of the variety of structures tested are shown on the right hand side of the figure.

Long-range Effects

In order to evaluate the effect of explicitly incorporating long range effects into the model structural properties (RDFs) of the 2.48 mol/kg NaCl solution were computed. These are compared to the short range model in Figure S6. Both predictions are in very good agreement for all cases of water, ions and ion-water RDFs. Nevertheless small discrepancies between long- and short-range model predictions in the cases of the Cl-Cl and Na-Cl RDFs prompt us to use the long-range model for production runs, given the additional physical information included in the model. In general however this analysis suggests that overall for our simulated systems, long-range effects do not have a substantial impact.

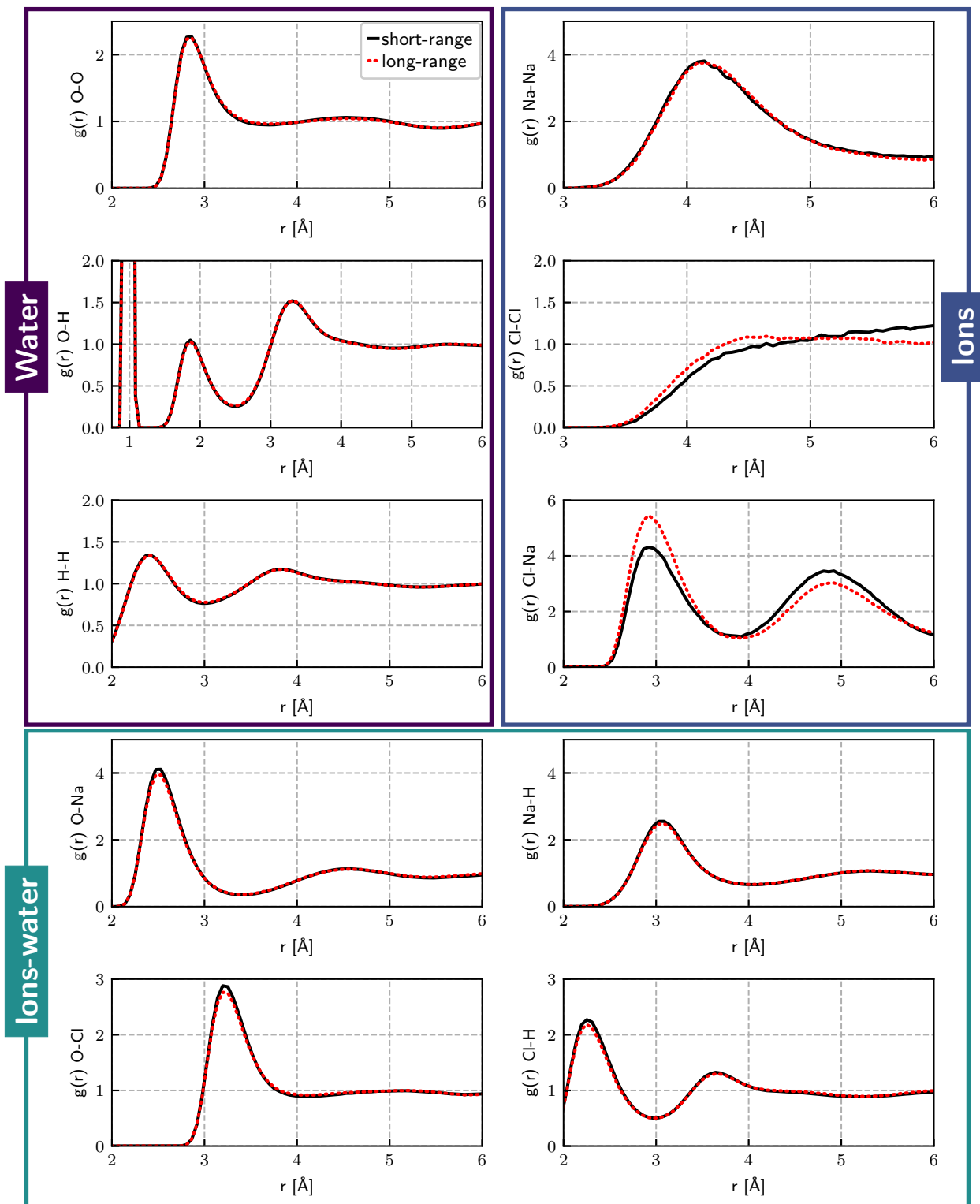


FIG. S6. Comparison of long and short-range models in predicting NaCl solution properties. RDFs for 2.48 mol/kg NaCl solution for both long- and short-range model predictions are shown in red and black respectively.

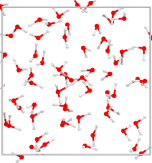
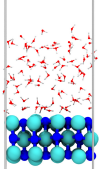
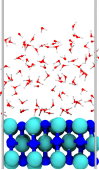
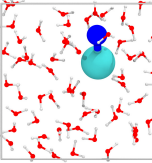
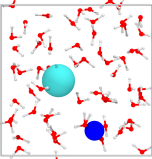
In summary this set of validation tests confirm the overall quality and accuracy of the C-NNP model. The model has performed comparably to or exceeded literature values on a variety of systems and properties that are very relevant for the dissolution process, from small scale studies of single ions in solution to systems sizes and interactions that will be explored in the detailed analysis of the dissolution process.

S3. MOLECULAR DYNAMICS SIMULATIONS

System setups

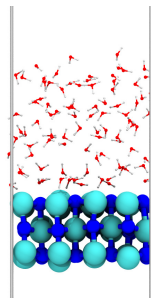
All simulations were carried out in an orthorhombic simulation cell with periodic boundary conditions in x, y, z directions. Details of the simulation setups for all systems are shown in Table ??.

TABLE II: Details of systems simulated. L is (unless stated) the cubic box dimensions in Å.

System	Simulation Details	Snapshot
Bulk H ₂ O	$N_{\text{water}} = 64$ $L = 12.42 \text{ \AA}$	
Na ⁺ / H ₂ O	$N_{\text{water}} = 63$ $N_{\text{Na}} = 1$ $L = 12.42 \text{ \AA}$	
Cl ⁻ / H ₂ O	$N_{\text{water}} = 63$ $N_{\text{Cl}} = 1$ $L = 12.42 \text{ \AA}$	
Na ⁺ -Cl ⁻ contact ion pair	$N_{\text{water}} = 62$ $N_{\text{Na}} = 1$ $N_{\text{Cl}} = 1$ $L = 12.42 \text{ \AA}$	
Na ⁺ -Cl ⁻ solvent-separated ion pair	$N_{\text{water}} = 62$ $N_{\text{Na}} = 1$ $N_{\text{Cl}} = 1$ $L = 12.42 \text{ \AA}$	

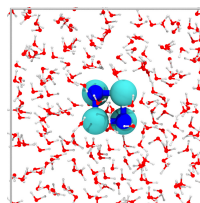
NaCl / H₂O interface

$$\begin{aligned} N_{\text{water}} &= 89 \\ N_{\text{Na}} &= 36 \\ N_{\text{Cl}} &= 36 \\ L(x,y,z) &= (16.2, 12.1, 58.7) \text{ \AA} \end{aligned}$$



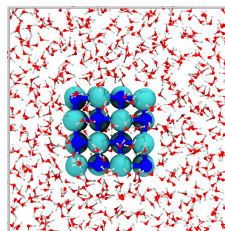
2 × 2 × 2 NaCl nanocrystal

$$\begin{aligned} N_{\text{water}} &= 229 \\ N_{\text{Na}} &= 4 \\ N_{\text{Cl}} &= 4 \\ L &= 19.8 \text{ \AA} \end{aligned}$$



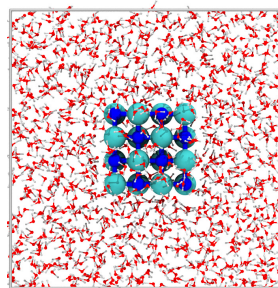
4 × 4 × 4 NaCl nanocrystal (2.48 mol/kg)

$$\begin{aligned} N_{\text{water}} &= 625 \\ N_{\text{Na}} &= 32 \\ N_{\text{Cl}} &= 32 \\ L &= 27.8 \text{ \AA} \end{aligned}$$



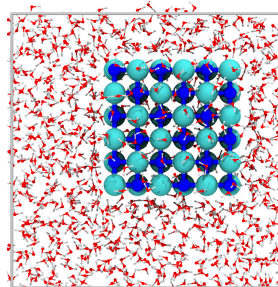
4 × 4 × 4 NaCl nanocrystal (1.42 mol/kg)

$$\begin{aligned} N_{\text{water}} &= 1250 \\ N_{\text{Na}} &= 32 \\ N_{\text{Cl}} &= 32 \\ L &= 34.1 \text{ \AA} \end{aligned}$$



6 × 6 × 6 NaCl nanocrystal (5.61 mol/kg)

$$\begin{aligned} N_{\text{water}} &= 1068 \\ N_{\text{Na}} &= 108 \\ N_{\text{Cl}} &= 108 \\ L &= 34.1 \text{ \AA} \end{aligned}$$



Simulation details

All MD/AIMD simulations were performed using the CP2K/Quickstep code.^{S19} AIMD simulations were used to generate reference data for development of the model as shown in Table III, with pre-equilibrated structures obtained from force field simulation. C-NNP

TABLE III. Details of simulation lengths performed with AIMD.

AIMD	
System	T_{sim}
Bulk H2O	100 ps
Na / H2O	80 ps
Cl / H2O	70 ps
NaCl/H2O interface	70 ps
Na-Cl contact ion pair	36 ps
Na-Cl solvent-separated ion pair	36 ps
2 x 2 x 2 NaCl nanocrystal	25 ps

TABLE IV. Details of simulation lengths for production runs performed with C-NNP.

C-NNP Production	
System	T_{sim}
4 × 4 × 4 NaCl nanocrystal (2.84 mol/kg)	10 × >2 ns
4 × 4 × 4 NaCl nanocrystal (1.42 mol/kg)	10 × >2 ns
6 × 6 × 6 NaCl nanocrystal (5.61 mol/kg)	10 × 10 - 30 ns

production simulations as shown in Table IV were initially equilibrated with fixed ions using the C-NNP model.

Force field pre-equilibration details

A 1 ns force-field based MD simulation was first performed on all Na/Cl containing systems from Table III to obtain a pre-equilibrated initial configuration for subsequent AIMD simulations. The Born-Mayer-Huggins potential for NaCl^{S20} and TIP3P model for water^{S17} were used and the water/NaCl interactions were described by the parameters given by Lynden-Bell et al. in Ref. S21.

Additional production simulations as described in Section S5 were performed using the Joung Cheatham (JC) model for ion-ion interactions, with SPC/E water model and ion-water interactions described by LJ crossed interactions using the Lorentz-Berthelot combination rules. These parameters were taken from Ref. S22.

AIMD simulation details

Prior to all AIMD simulations, a short constrained AIMD simulation, keeping ions fixed, was performed on all the systems given in Table III containing ions, to obtain a well-equilibrated water structure around the Na and Cl ions. These were used as starting configurations for simulations in NVT ensemble within the generalised gradient approximation using the revPBE functional^{S4} with Grimmes’ dispersion correction.^{S23} The electronic density was partitioned into core and valence contributions, with core electrons described using the norm-conserving Goedecker, Teter and Hutter (GTH) pseudopotentials.^{S24} Na 2s and 2p electrons were also treated explicitly given the well-known issue of non-linear core-valence exchange/correlation. Valence electrons were described using the MOLOPT TZV2P basis set.^{S25} Stochastic errors for Na forces due to insufficient basis set convergence were observed in additional DFT convergence tests for the cutoff of the plane-wave representation of the charge density. Therefore a plane wave cutoff of 1200 Ry was used to obtain accurate forces. Deuterium masses were used in lieu of hydrogen, allowing a 1 fs timestep and reducing errors due to neglecting nuclear quantum effects through classical propagation of the nuclei. Simulations were performed at 300 K, maintained using the CSV thermostat..^{S26} All AIMD simulations were at least 40 ps long (except for $2 \times 2 \times 2$ NaCl nanocrystal which was 25 ps due to computational cost.) and can be found in Table III.

S4. ANALYSIS DETAILS

Steinhardt order parameters

The Steinhardt order parameter q_8 is a particular case of a larger set of bond order parameters based on spherical harmonics.^{S27} To distinguish between solid and liquid-like ions we first compute the complex vector $q_8(i)$ for each particle i , where $N_b(i)$ is the number of nearest neighbours of particle i , and m runs from -8 to +8.

$$q_{8,m}(i) = \frac{1}{N_b(i)} \sum_j^{N_b(i)} Y_{8,m}(\mathbf{r}_{i,j}) \quad (\text{S1})$$

$Y_{8,m}$ are the spherical harmonics and $\mathbf{r}_{i,j}$ connects particles i and j . Following Lechner et al.^{S28} we then compute an averaged form of this local bond order parameter by averaging the local $q_{8,m}(i)$ vectors over the particle i and its surroundings:

$$\bar{q}_8(i) = \sqrt{\frac{4\pi}{2l+1} \sum_{m=-l}^l |q_{8,m}(i)|^2} \quad (\text{S2})$$

where

$$\bar{q}_{8,m}(i) = \frac{1}{\tilde{N}_b(i)} \sum_{k=0}^{\tilde{N}_b(i)} Y_{8,m}(k) \quad (\text{S3})$$

and $\tilde{N}_b(i)$ are the neighbours of particle i

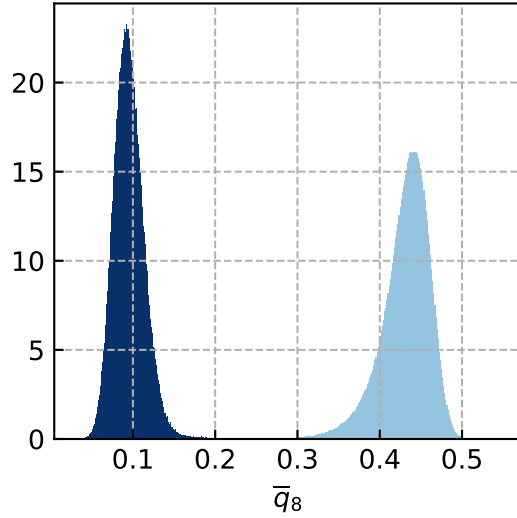


FIG. S7. \bar{q}_8 distributions for ideal cases of pristine NaCl lattice (light blue) and solvated Na/Cl ions (dark blue).

Computation of these bond order parameters was performed using the Freud^{S29} python package.

Coordination Numbers and clusters

Computation of all coordination numbers and clusters were performed using Plumed,^{S30} and analysis carried out using Python. The CN of an atom i with a set of atoms in A is

defined by:

$$\text{CN}_i = \sum_{j \in A} s_{ij} \tag{S4}$$

where s_{ij} is a smooth switching function with a range of [0,1]:

$$s_{ij} = \left(\frac{1 - \left(\frac{r_{ij}}{r_0}\right)^6}{1 - \left(\frac{r_{ij}}{r_0}\right)^{12}} \right) \tag{S5}$$

r_{ij} is the interatomic distance between atom i and atom j . r_0 for Na-O (2.80 Å) and Cl-H (2.60 Å) were obtained from literature values,^{S31} while r_0 for Na-Cl was taken such that the CNs of the pristine lattice coincided with the integral up to the first minimum of the Na-Cl RDF (3.5 Å). An ion was defined as dissolved if it has a Na-O/Cl-H CN less than 1 for more than 8 ps. We show that this definition is not sensitive to changes in the time chosen in Figure S8. The cluster size distributions were computed by detecting coordinated ions

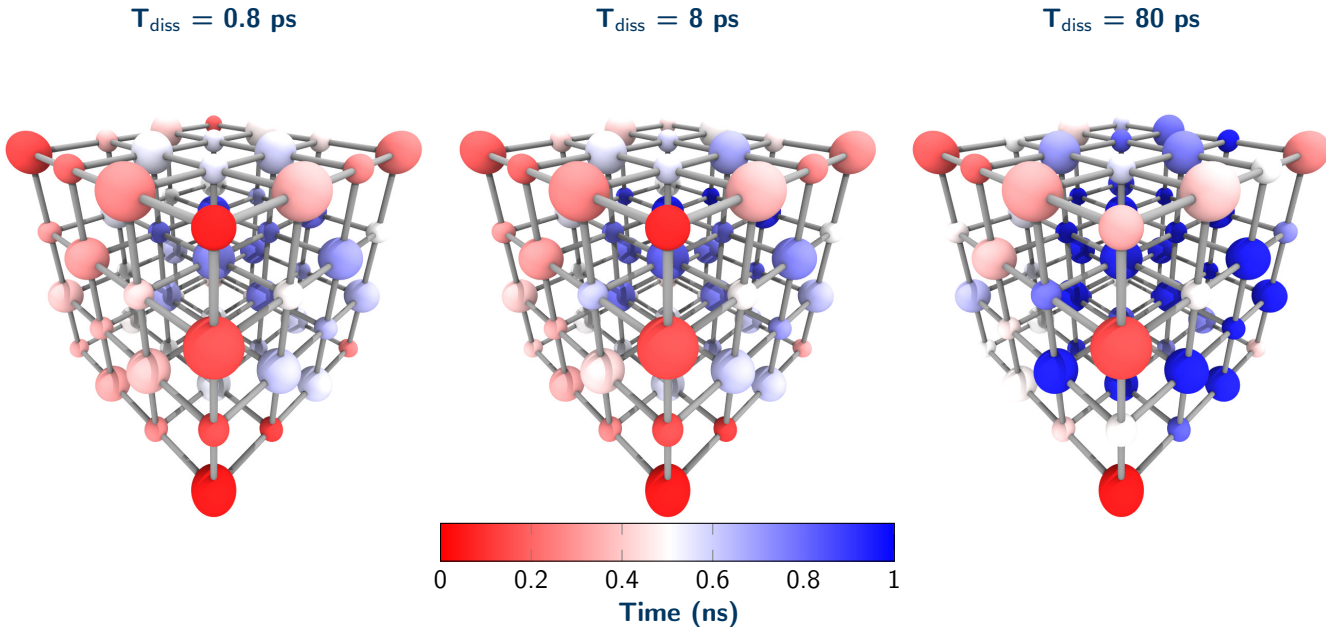


FIG. S8. Sensitivity of dissolution behaviour of ions based on definition of time spent with $\text{CN} < 1$.

using a threshold of a ion-ion $\text{CN} > 2$, and then using these atoms as input for a depth first search graph reduction algorithm to identify the sets of ions clustered together.

To compute the surface area to volume ratio of the dissolving crystal, a DFS algorithm was implemented using the Freud Python package^{S29} in order to identify the ions in the

largest cluster at a given time. The convex hull of this set of points was then obtained (provided there were > 3 ions in the cluster), and the surface area to volume ratio of the hull was computed.

S5. ADDITIONAL RESULTS

MLP

Results from identical simulations as described above for the C-NNP at 2.48 mol/kg NaCl concentration at 400 K are shown in Figure S9. The additional results for the 1.42 mol/kg and 2.48 mol/kg trajectories at 330 K are also shown in Figure S9.

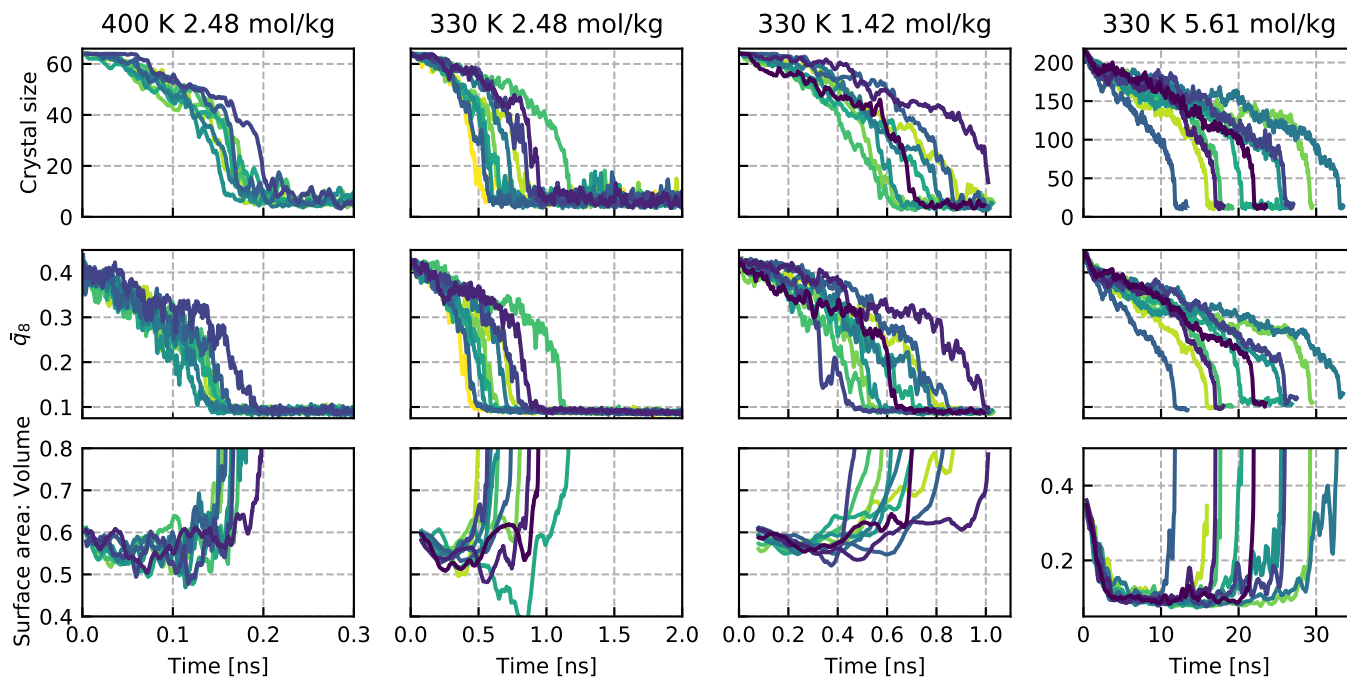


FIG. S9. Crystal size, \bar{q}_8 and surface area:volume ratio for ten simulated trajectories at 400 K (2.48 mol/kg) and 330 K (2.48 mol/kg, 1.42 mol/kg and 5.61 mol/kg).

FF

Results from identical simulations as described above for the C-NNP at 1.42 mol/kg and 2.48 mol/kg at 330 K are shown in Figure S10 for a JC/SCP/E force-field model.

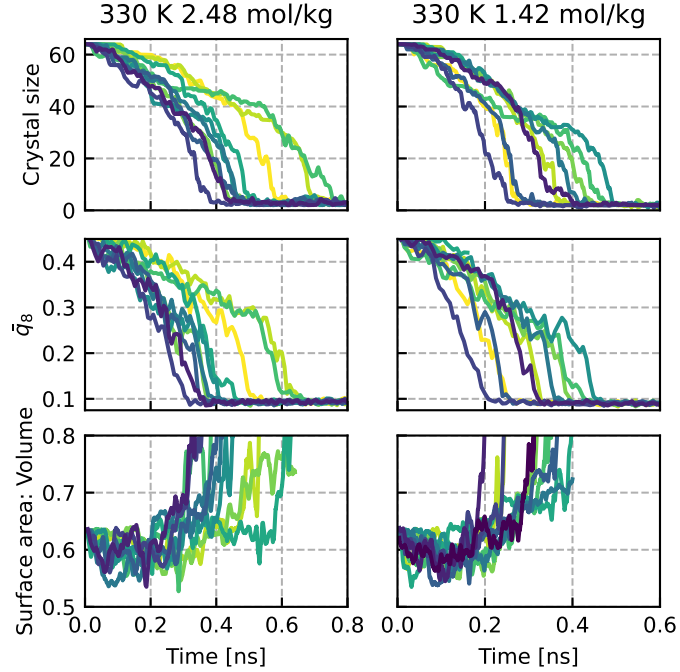


FIG. S10. Crystal size, \bar{q}_8 and surface area:volume ratio for ten simulated trajectories with JC/SPC/E at 330 K (2.48 mol/kg and 1.42 mol/kg).

REFERENCES

REFERENCES

- ^{S1}L. Zheng, M. Chen, Z. Sun, H. Y. Ko, B. Santra, P. Dhuvad, and X. Wu, “Structural, electronic, and dynamical properties of liquid water by ab initio molecular dynamics based on SCAN functional within the canonical ensemble,” *J. Chem. Phys.* **148**, 164505 (2018).
- ^{S2}M. Galib, T. T. Duignan, Y. Misteli, M. D. Baer, G. K. Schenter, J. Hutter, and C. J. Mundy, “Mass density fluctuations in quantum and classical descriptions of liquid water,” *J. Chem. Phys.* **146**, 244501 (2017).
- ^{S3}J. P. Perdew, K. Burke, and M. Ernzerhof, “Generalized Gradient Approximation Made Simple,” *Phys. Rev. Lett.* **77**, 3865–3868 (1996).
- ^{S4}Y. Zhang and W. Yang, “Comment on “Generalized Gradient Approximation Made Simple”,” *Phys. Rev. Lett.* **80**, 890 (1998).
- ^{S5}J. Sun, A. Ruzsinszky, and J. Perdew, “Strongly Constrained and Appropriately Normed Semilocal Density Functional,” *Phys. Rev. Lett.* **115**, 036402 (2015).

- ^{S6}O. Marsalek and T. E. Markland, “Quantum Dynamics and Spectroscopy of Ab Initio Liquid Water: The Interplay of Nuclear and Electronic Quantum Effects,” *J. Phys. Chem. Lett.* **8**, 1545–1551 (2017).
- ^{S7}A. P. Gaiduk, J. Gustafson, F. Gygi, and G. Galli, “First-Principles Simulations of Liquid Water Using a Dielectric-Dependent Hybrid Functional,” *J. Phys. Chem. Lett.* **9**, 3068–3073 (2018).
- ^{S8}T. T. Duignan, G. K. Schenter, J. L. Fulton, T. Huthwelker, M. Balasubramanian, M. Galib, M. D. Baer, J. Wilhelm, J. Hutter, M. Del Ben, X. S. Zhao, and C. J. Mundy, “Quantifying the hydration structure of sodium and potassium ions: Taking additional steps on Jacob’s Ladder,” *Phys. Chem. Chem. Phys.* **22**, 10641–10652 (2020).
- ^{S9}A. K. Soper and K. Weckström, “Ion solvation and water structure in potassium halide aqueous solutions,” *Biophys. Chem.* **124**, 180–191 (2006).
- ^{S10}L. B. Skinner, C. Huang, D. Schlesinger, L. G. Pettersson, A. Nilsson, and C. J. Benmore, “Benchmark oxygen-oxygen pair-distribution function of ambient water from x-ray diffraction measurements with a wide Q-range,” *J. Chem. Phys.* **138**, 074506 (2013).
- ^{S11}J. Wiktor, F. Ambrosio, and A. Pasquarello, “Note: Assessment of the SCAN+rVV10 functional for the structure of liquid water,” *J. Chem. Phys.* **147**, 164505 (2017).
- ^{S12}C. Schran, F. L. Thiemann, P. Rowe, E. A. Müller, O. Marsalek, and A. Michaelides, “Machine learning potentials for complex aqueous systems made simple,” *Proc. Natl. Acad. Sci. U. S. A.* **118** (2021).
- ^{S13}C. Schran, K. Brezina, and O. Marsalek, “Committee neural network potentials control generalization errors and enable active learning,” *J. Chem. Phys.* **153**, 104105 (2020).
- ^{S14}T. Morawietz, A. Singraber, C. Dellago, and J. Behler, “How van der Waals interactions determine the unique properties of water,” *Proc. Natl. Acad. Sci.* **113**, 8368–8373 (2016).
- ^{S15}J. Behler, “Atom-centered symmetry functions for constructing high-dimensional neural network potentials,” *J. Chem. Phys.* **134**, 74106 (2011).
- ^{S16}A. Singraber, T. Morawietz, J. Behler, and C. Dellago, “Parallel Multistream Training of High-Dimensional Neural Network Potentials,” *J. Chem. Theory Comput.* **15**, 3075–3092 (2019).
- ^{S17}W. L. Jorgensen, J. Chandrasekhar, J. D. Madura, R. W. Impey, and M. L. Klein, “Comparison of simple potential functions for simulating liquid water,” *J. Chem. Phys.* **79**, 926–935 (1983).

- ^{S18}V. Quaranta, M. Hellström, and J. Behler, “Proton-Transfer Mechanisms at the Water-ZnO Interface: The Role of Presolvation,” *J. Phys. Chem. Lett.* **8**, 1476–1483 (2017).
- ^{S19}T. D. Kühne, M. Iannuzzi, M. Del Ben, V. V. Rybkin, P. Seewald, F. Stein, T. Laino, R. Z. Khaliullin, O. Schütt, F. Schiffmann, D. Golze, J. Wilhelm, S. Chulkov, M. H. Bani-Hashemian, V. Weber, U. Borštnik, M. Taillefumier, A. S. Jakobovits, A. Lazzaro, H. Pabst, T. Müller, R. Schade, M. Guidon, S. Andermatt, N. Holmberg, G. K. Schenter, A. Hehn, A. Bussy, F. Belleflamme, G. Tabacchi, A. Glöß, M. Lass, I. Bethune, C. J. Mundy, C. Plessl, M. Watkins, J. VandeVondele, M. Krack, and J. Hutter, “CP2K: An electronic structure and molecular dynamics software package - Quickstep: Efficient and accurate electronic structure calculations,” *J. Chem. Phys.* **152**, 194103 (2020).
- ^{S20}F. G. Fumi and M. P. Tosi, “Ionic sizes and born repulsive parameters in the NaCl-type alkali halides—I: The Huggins-Mayer and Pauling forms,” *J. Phys. Chem. Solids* **25**, 31–43 (1964).
- ^{S21}R. M. Lynden-Bell and J. C. Rasaiah, “From hydrophobic to hydrophilic behaviour: A simulation study of solvation entropy and free energy of simple solutes,” *J. Chem. Phys.* **107**, 1981–1991 (1997).
- ^{S22}A. L. Benavides, J. L. Aragoñes, and C. Vega, “Consensus on the solubility of NaCl in water from computer simulations using the chemical potential route,” *The Journal of Chemical Physics* **144**, 124504 (2016).
- ^{S23}S. Grimme, J. Antony, S. Ehrlich, and H. Krieg, “A consistent and accurate ab initio parametrization of density functional dispersion correction (DFT-D) for the 94 elements H-Pu,” *J. Chem. Phys.* **132**, 154104 (2010).
- ^{S24}S. Goedecker, M. Teter, and J. Hutter, “Separable dual-space Gaussian pseudopotentials,” *Phys. Rev. B* **54**, 1703–1710 (1996).
- ^{S25}J. VandeVondele and J. Hutter, “Gaussian basis sets for accurate calculations on molecular systems in gas and condensed phases,” *J. Chem. Phys.* **127**, 114105 (2007).
- ^{S26}G. Bussi, D. Donadio, and M. Parrinello, “Canonical sampling through velocity rescaling,” *J. Chem. Phys.* **126**, 14101 (2007).
- ^{S27}P. J. Steinhardt, D. R. Nelson, and M. Ronchetti, “Bond-orientational order in liquids and glasses,” *Phys. Rev. B* **28**, 784–805 (1983).
- ^{S28}W. Lechner and C. Dellago, “Accurate determination of crystal structures based on averaged local bond order parameters,” *J. Chem. Phys.* **129**, 114707 (2008).

- ^{S29}V. Ramasubramani, B. D. Dice, E. S. Harper, M. P. Spellings, J. A. Anderson, and S. C. Glotzer, “freud: A software suite for high throughput analysis of particle simulation data,” *Comput. Phys. Commun.* **254**, 107275 (2020).
- ^{S30}M. Bonomi, G. Bussi, C. Camilloni, G. A. Tribello, P. Banáš, A. Barducci, M. Bernetti, P. G. Bolhuis, S. Bottaro, D. Branduardi, R. Capelli, P. Carloni, M. Ceriotti, A. Cesari, H. Chen, W. Chen, F. Colizzi, S. De, M. De La Pierre, D. Donadio, V. Drobot, B. Ensing, A. L. Ferguson, M. Filizola, J. S. Fraser, H. Fu, P. Gasparotto, F. L. Gervasio, F. Giberti, A. Gil-Ley, T. Giorgino, G. T. Heller, G. M. Hocky, M. Iannuzzi, M. Invernizzi, K. E. Jelfs, A. Jussupow, E. Kirilin, A. Laio, V. Limongelli, K. Lindorff-Larsen, T. Löhr, F. Marinelli, L. Martin-Samos, M. Masetti, R. Meyer, A. Michaelides, C. Molteni, T. Morishita, M. Nava, C. Paissoni, E. Papaleo, M. Parrinello, J. Pfaendtner, P. Piaggi, G. M. Piccini, A. Pietropaolo, F. Pietrucci, S. Pipolo, D. Provasi, D. Quigley, P. Raiteri, S. Raniolo, J. Rydzewski, M. Salvalaglio, G. C. Sosso, V. Spiwok, J. Šponer, D. W. Swenson, P. Tiwary, O. Valsson, M. Vendruscolo, G. A. Voth, and A. White, “Promoting transparency and reproducibility in enhanced molecular simulations,” *Nat. Methods* **16**, 670–673 (2019).
- ^{S31}L.-M. Liu, A. Laio, and A. Michaelides, “Initial stages of salt crystal dissolution determined with ab initio molecular dynamics,” *Phys. Chem. Chem. Phys.* **13**, 13162–13166 (2011).